

# Towards modelling of fluid flow and food breakage by the teeth in the oral cavity using smoothed particle hydrodynamics (SPH)

Simon M. Harrison · Paul W. Cleary

Received: 13 December 2012 / Revised: 29 July 2013 / Accepted: 9 August 2013 / Published online: 27 September 2013  
© Springer-Verlag Berlin Heidelberg 2013

**Abstract** The mechanical functions of the oral cavity, such as chewing and swallowing, present many modelling challenges. Plastic strain and fracturing occur in food due to interactions with hard and soft tissues, whilst the food moves, collides and mixes with fluid. Smoothed particle hydrodynamics (SPH) is a meshless numerical method that uses particles instead of meshes to discretise material. The Lagrangian nature of SPH means that it is well suited to modelling complexities such as fluid-free surfaces or solid fracture, interactions with complicated deforming boundaries, and temperature and chemical dynamics. We propose a combined SPH–biomechanical model of the oral cavity and present five model applications that address a broad range of material behaviours observed during eating. Interactions between the gums, teeth and the moving tongue with fluids in the anterior oral cavity; biting and chewing of elastoplastic foods; and biting and crushing of brittle foods are each simulated. In each case, the proposed meshless SPH–biomechanical model was found to be well suited to modelling the complex motions, boundary interactions and material responses. The modelling framework shows promise as a tool for simulation of food breakdown and taste release for foods of different material behaviours.

**Keywords** Computational fluid dynamics (CFD) · SPH · Mouth · Tongue · Saliva · Food · Mastication · Biomechanics

## Introduction

Despite the oral cavity's importance in performing duties that sustain life, namely chewing, swallowing and breathing, few studies have focused on the mechanical modelling of its functions. The physics of chewing and swallowing of food involves the coupling of the damage mechanics of solids, the fluid mechanics of saliva and liquid food, the formation of pastes and the interactions between muscular contraction and the soft tissue of the mouth. Modelling of these coupled processes poses a significant challenge and motivates the development of techniques that can accurately represent these phenomena.

The mechanical behaviour of food is intrinsically linked to our sensory experience of eating. Our experience of taste for liquid food is more sensitive than that for solid food [41], and the manner in which food breaks down in the mouth affects how we perceive sensory properties of food. The texture of food contributes to a sensory experience separate from that of taste [102]. The relationship of the rheological properties of food with their textural sensation during consumption has been investigated using 2D analytical models [12, 40, 62]. However, many critical aspects have not yet been directly modelled, such as the breakdown of different types of food by biting and chewing (which includes cutting, crushing and grinding processes), the interactions between the tongue, teeth and the soft tissue of the oral cavity during food breakdown, the release of taste and aroma compounds during breakdown and transport to the receptors, and the dissolution and lubrication of food by the saliva.

Mastication, whilst a continuous process, can be broken down into a number of distinct phases, with different modelling requirements. Ingestion begins the process, and this may include biting of a large piece of food by the incisors

S. M. Harrison (✉) · P. W. Cleary  
CSIRO Mathematics, Informatics and Statistics, Private Bag 33,  
Clayton South, VIC 3169, Australia  
e-mail: Simon.Harrison@csiro.au

or submolars, which is subsequently placed between the molars for the next phase. When simulating the ingestion of liquid food, the transient flow of the liquid and the interactions between the liquid and anatomical features must be considered. In the case of solid food, an ingestion model must consider elastic, plastic and brittle material behaviour and the simulation must track interactions with the oral cavity as well as the trajectories of food fragments.

Early-stage chewing progresses next, during which the molars crush and grind the food and the tongue relocates the food fragments for the next chewing cycle. The simulation technique must again consider elastic–plastic–brittle material behaviour and interactions between the food, teeth and tongue all of which move and deform dynamically. Saliva is progressively mixed into the comminuted food, at a rate depending on the properties of the food and many attributes of the individual. Mixing of the saliva with the food causes lubrication, agglomeration and changes to the properties of the food (e.g. softening by wetting). As the food softens (or if the food was soft to begin with), the tongue may also crush the food between itself and the upper palate. Multiple phases must then be modelled as well as the compliance of the tongue and other soft tissues. Taste and aroma compounds are released from the food and are transported to receptors during these stages. Advection and diffusion models are required to track the transport of these flavour compounds. In later-stage mastication and swallowing, the food is formed into a bolus and transported towards the oropharynx. The pulsatory motion of the tongue and its interactions with other soft tissues must be modelled as they push the food into the oesophagus. Few studies present models of the individual features of mastication listed above, and no model has yet been presented that encompasses all aspects of mastication.

Few studies have simulated liquids in the oral cavity. Nicosia and Robbins [79] used a 2D computational fluid dynamics (CFD) model to look at the effect of bolus viscosity and density on the time taken during swallowing. Mathmann et al. [73] used a 3D CFD model to study the effect of yogurt viscosity on fluid velocity induced by contact between an idealised tongue and soft palate. In both cases, they assumed that the tongue and soft palate could be represented as rigid bodies and used simplified kinematics to model contraction of the tongue musculature. The bolus was modelled as a homogeneous viscous fluid in both cases. Results were intuitive, for example, Nicosia and Robbins found that the time taken to swallow depended on bolus viscosity (or bolus density if the viscosity was small), but the strong assumptions made in the development of the model limit the validity of the numerical results. The tongue (and, to a lesser degree, the soft palate) deforms in three dimensions during swallowing. Also, the bolus may be a heterogeneous mixture of solid and liquid food and

saliva. More work is required to develop realistic models of fluid flow in the mouth for processes such as dissolution of solid food, sloshing of saliva and other liquids during jaw movement and swallowing.

Musculoskeletal modelling of constrained jaw movement has elucidated the role of muscles in generating force at the teeth surfaces during biting, but detailed models of the interaction between food and the mouth (specifically the teeth, jaw, gums and tongue) during realistic chewing have not yet been reported. Some studies use control theory to reproduce the rigid-body kinematics of the jaw [106]. Some 3D finite element (FE)-based models have been developed to predict stresses in the jaw bones and teeth [63, 64, 89] from calculations of muscle force. However, the interaction between food and the teeth in these models was represented by simple kinematic constraints, i.e. by specifying either the translations of the jaw joint or local displacements at the surface of one tooth. An understanding of the loading on the teeth reasonably requires the modelling of food response as chewing progresses. For instance, it is known that jaw kinematics varies with the material properties of food [11, 30, 65, 83]. Therefore, it is likely that the kinematics and kinetics of chewing will change as the material properties and geometric attributes of the food change.

Only Dejak et al. [39], Amemiya et al. [3] and Sun and Xu [94] have modelled interaction between teeth and some form of idealised food. Dejak et al. studied the stresses resulting in the teeth during chewing using a 2D FE model of the compression of elastic solids by the first molars. The teeth were represented by idealised geometries that were partitioned by material type into single areas of enamel, dentin and periodontium. Independent material properties were assigned to each of these regions. Food morsels were modelled as perfectly elastic solids of rectangular shape. Material properties were chosen to represent hard gum, tough meat, bone and a portion of hard gum with a small piece of embedded bone. Teeth clenching and mastication were modelled using a combination of prescribed displacement and load. The locations of high stress in the teeth were found to depend on the material properties of the food morsel. However, damage of the food, such as by fracture or plastic deformation, was not included. The elastic food models supplied a plausible distributed load on the teeth contact surfaces for the prediction of internal teeth stresses rather than providing the rheological details of the evolution of food structure during chewing. Amemiya et al. [3] modelled bolus occlusion between a single top and bottom molar in three dimensions, using a viscoelastic material model, measured jaw kinematics and the FE method. The viscoelastic material model included parameters allowing variation in mechanical response due to mixing with saliva at an assumed rate. Whilst this model was able to simulate

cumulative changes in bolus shape after cycles of chewing, the viscoelastic material model used did not explicitly predict fracture damage or plastic strain in foodstuffs and so may be limited in validity.

Sun and Xu [94] proposed the use of the discrete element method (DEM) to study the breakdown and transport of food during mastication and swallowing. Simple models of chewing and swallowing were presented to indicate the applicability of the DEM method to this application. The models were implemented using Particle Flow Code in two Dimensions (PFC<sup>2D</sup> 3.1, ITASCA) software. Break-up of the food was studied using mathematical models of contact, slip and separation and particle bonding. The particle bonding model assumed constant bond strength. Swallowing was modelled using idealised, rigid geometries of the tongue, palate and oesophagus. The palate was able to rotate in the sagittal plane to accommodate transport of a bolus through the oral cavity. In both cases, the geometries, kinematics and material properties were highly simplified, and no quantitative measures were presented. To date, there has been no three-dimensional modelling of chewing that incorporates realistic breakdown of food or deformation of soft tissues.

The creation of a comprehensive model of mastication is a task that is too large to complete in one study. We propose a new 3D model with coupled fluid flow, elastic and plastic solid deformation including the break-up of food, realistic jaw dynamics, tongue motion and soft tissue interactions based on a combination of the smoothed particle hydrodynamics (SPH) and biomechanics models. In this paper, we demonstrate the applicability of such a modelling framework to several key aspects of early mastication by modelling five key processes:

1. Fluid (saliva and/or liquid food) motion in the anterior oral cavity induced by inertia, gravity and interaction with the tongue, gums and teeth.
2. Cutting of an elastoplastic model “jelly bean” by the incisors.
3. Chewing of an elastoplastic model “jelly baby” by the molars performing realistic grinding motion.
4. Fracturing of a brittle piece of candy during biting by the incisors
5. Fracturing and break-up of a brittle piece of candy during crushing between molars.

These examples highlight some of the knowledge that can be gained from 3D mechanical modelling of the oral cavity and possible future directions of such techniques. By the use of examples from the literature, we also explain how a coupled SPH–biomechanical model may be able to simulate the features of latter-stage chewing and swallowing in future work.

## Numerical method

SPH is a numerical method for solving partial differential equations (PDEs). It is a meshless Lagrangian method in which the governing equations are solved on a moving set of particles that represent discretised volumes of material. See Monaghan [76] and Cleary [15] for detailed explanations of the method and reviews by Monaghan [78] and Gomez-Gesteira et al. [46]. It has been used extensively to simulate industrial fluid flows [24, 25] and to predict geophysical and extreme flow events in 2D [36] and in 3D [19, 55]. It has also been shown to be useful for applications such as multi-phase flows with coarse solids and interstitial fluid [85, 86], explosions and impacts [70, 92, 95], high-pressure die casting [20–22] and ingot casting [85, 86], metal forging and extrusion [23], liquid sloshing [49], viscoelastic flow [42] and the dynamics of elastoplastic solids [14, 16, 48] and elastic–brittle fracture [31, 32].

SPH is suited to fluid applications where complex free surfaces occur or for solid mechanics applications where large deformations and damage occur. Unlike more traditional methods such as finite-volume and finite-element analyses that represent material with meshes, SPH particles represent specific volumes of material and move at the material velocity. These particles carry information about physical properties of the system such as pressure, density, velocity and stresses. Forces between particles are determined using a smoothing kernel function and are dependent on the distance between the particles. The use of the kernel function allows the governing partial differential equations (PDEs) of the physical system to be converted into spatially discretised systems of ordinary differential equations (ODEs), which can then be integrated forward in time to predict the state of the system. The SPH equations of motion for fluids, elastic solids, elastoplastic solids and brittle solids are summarised below.

The SPH formulation for fluids

The SPH continuity equation for fluids given by Monaghan [76] in a form suitable for predicting free-surface flows is:

$$\frac{d\rho_a}{dt} = \sum_b m_b \mathbf{v}_{ab} \cdot \nabla_a W_{ab} \quad (1)$$

where  $\rho_a$  is the density of particle  $a$ ,  $t$  is time, and  $m_b$  is the mass of particle  $b$ , where  $\mathbf{v}_{ab} = \mathbf{v}_a - \mathbf{v}_b$  and  $\mathbf{v}_a$  and  $\mathbf{v}_b$  are the velocities of particles  $a$  and  $b$ .  $W$  is a cubic interpolation kernel function that is evaluated for the distance (magnitude of the vector  $\mathbf{r}_{ab}$ ) between particles  $a$  and  $b$ . The kernel function is given in and its properties are described in Monaghan [78].

Conservation of momentum in the SPH formulation results in the following acceleration Eq. [15]:

$$\frac{d\mathbf{v}_a}{dt} = - \sum_b m_b \left[ \left( \frac{P_b}{\rho_b^2} + \frac{P_a}{\rho_a^2} \right) - \frac{\xi}{\rho_a \rho_b} \frac{4\mu_a \mu_b}{(\mu_a + \mu_b)} \frac{\mathbf{v}_{ab} \cdot \mathbf{r}_{ab}}{\mathbf{r}_{ab}^2 + \eta^2} \right] \times \nabla_b W_{ab} + \mathbf{g} \tag{2}$$

where  $P_a$  and  $\mu_a$  are the local pressure and dynamic viscosity for particle  $a$ , respectively,  $\eta$  is a small number to mitigate singularities,  $\xi$  is a normalisation constant for the kernel function, and  $\mathbf{g}$  is the gravitational acceleration.

A quasi-compressible formulation of the SPH method is employed. The equation of state for weakly compressible fluids relates the particle density,  $\rho$ , and the fluid pressure,  $P$ :

$$P = P_0 \left[ \left( \frac{\rho}{\rho_0} \right)^\gamma - 1 \right] \tag{3}$$

where  $\gamma$  is a material constant, which is equal to 7 for fluids with properties similar to water [5], the reference density is given by  $\rho_0$ , and  $P_0$  prescribes the overall dynamic pressure scale, which is given by:

$$\frac{\gamma P_0}{\rho_0} = 100V^2 = c^2 \tag{4}$$

where  $V$  is the maximum fluid velocity and  $c$  is the speed of sound.

A second-order predictor–corrector integration scheme is used [76] with time step chosen so that it satisfies the Courant condition with a modification for the presence of viscosity (see [15]):

$$\delta t = \min_a \left( 0.5 \cdot h / \left( c + \frac{2\xi\mu_a}{h\rho_a} \right) \right) \tag{5}$$

where  $h$  is the smoothing length of the kernel.

The SPH formulation for elastoplastic and brittle solids

The SPH continuity equation for solid materials is the same as for fluids (1). Conservation of momentum for solids results in the following acceleration equation [68]:

$$\frac{d\mathbf{v}_a}{dt} = \sum_b m_b \left( \frac{\boldsymbol{\sigma}_a}{\rho_a^2} + \frac{\boldsymbol{\sigma}_b}{\rho_b^2} + \Pi_{ab}\mathbf{I} \right) \cdot \nabla_a W_{ab} + \mathbf{g} \tag{6}$$

where  $\boldsymbol{\sigma}_a$  and  $\boldsymbol{\sigma}_b$  are the stress tensors of particles  $a$  and  $b$ , respectively,  $\Pi_{ab}$  is an artificial representation of viscosity terms that result in both shear and bulk viscosity, and  $\mathbf{I}$  is the identity tensor. We use a linear elastic model for the solid rheology. This is given by the equation of state which relates the pressure to the density:

$$P = c^2 (\rho - \rho_0) \tag{7}$$

where  $\rho_0$  is the reference density. The speed of sound  $c$  in the solid material is given by:

$$c = \sqrt{K/\rho_0} \tag{8}$$

where  $K$  is the bulk modulus.

The stress tensor can be partitioned into a pressure term and a deviatoric stress term with tensor,  $\mathbf{S}$ :

$$\boldsymbol{\sigma} = -P\mathbf{I} + \mathbf{S} \tag{9}$$

From [48], the evolution of  $\mathbf{S}$  is given in component form as:

$$\frac{dS^{ij}}{dt} = 2G \left( \dot{\varepsilon}^{ij} - \frac{1}{3} \delta^{ij} \dot{\varepsilon}^{kk} \right) + S^{ik} \Omega^{jk} + \Omega^{ik} S^{kj} \tag{10}$$

where  $\dot{\varepsilon}$  is the strain tensor,  $\delta^{ij}$  is the Kronecker delta,  $\Omega^{jk}$  is the Jaumann rotation tensor,  $G$  is the shear modulus, and indices  $i, j$  and  $k$  refer to three orthogonal directions in 3D space.

The strain rate tensor is calculated in an SPH form as:

$$\dot{\varepsilon}_a = -\frac{1}{2} \sum_b \frac{m_b}{\rho_b} \left[ (\mathbf{v}_{ab} \nabla_a W_{ab})^T + \mathbf{v}_{ab} \nabla_a W_{ab} \right] \tag{11}$$

and the Jaumann rotation tensor is expressed as:

$$\Omega_a = \frac{1}{2} \sum_b \frac{m_b}{\rho_b} \left[ (\mathbf{v}_{ab} \nabla_a W_{ab})^T - \mathbf{v}_{ab} \nabla_a W_{ab} \right] \tag{12}$$

The SPH method, particularly for elastic solids, can display tensile instabilities [77]. The tensile instability correction proposed by Gray et al. [48] is used here with a coefficient of 0.3 to inhibit these instabilities. This choice follows detailed evaluation of the tensile correction for SPH modeling of elastic solids in uniaxial compression tests [33].

Again, a second-order predictor–corrector (explicit) integration scheme is used with time step chosen to satisfy the Courant condition:

$$\delta t = \frac{0.5 \cdot h}{c} \tag{13}$$

For elastoplastic solids, the radial return plasticity model [101] is used to track the extent of plastic deformation. At the beginning of a time step, a trial deviatoric stress,  $S_{T,r}^{ij}$ , is determined, assuming an elastic response. The resulting change in plastic strain,  $\varepsilon^p$ , is:

$$\Delta \varepsilon^p = \frac{\sigma_{vm} - \sigma_y}{3G + H} \tag{14}$$

where  $\sigma_{vm}$  is the von Mises stress,  $\sigma_y$  is the yield stress, and  $H$  is the hardening modulus. The plastic strain is then incremented:

$$\varepsilon^p = \varepsilon^p + \Delta \varepsilon^p \tag{15}$$

The yield stress increment at the end of the time step is determined:

$$\Delta\sigma_y = H \Delta\varepsilon^p \tag{16}$$

The deviatoric stress at the end of the time step,  $S^{ij}$ , is calculated from the trial deviatoric stress:

$$S^{ij} = r_s S_{Tr}^{ij} \tag{17}$$

where  $r_s$  is the radial scale factor:

$$r_s = \frac{\sigma_y}{\sigma_{ym}} \tag{18}$$

When brittle fracture is considered, a continuum damage law based on the model of Grady and Kipp [47] is applied. Following Benz and Asphaug [6], each SPH particle is assigned a damage parameter,  $D$ , which has a value between zero and unity and specifies the local extent of fracture. If larger than zero, this parameter reduces the transmission of tensile stress between adjacent particles (in all three dimensions).

In SPH the damage evolution is given by a differential form of the Grady–Kipp model:

$$\frac{dD^{1/3}}{dt} = \frac{(m + 3)}{3} \alpha^{1/3} \varepsilon^{1/3} \tag{19}$$

where  $\varepsilon$  is the tensile strain and  $\alpha$  is a constant that depends on the flaw density,  $k$ , the Weibull modulus,  $m$ , and the crack growth speed,  $C_g$ , and is given by:

$$\alpha = \frac{8\pi C_g^3 k}{(m + 1)(m + 2)(m + 3)} \tag{20}$$

This model was originally applied in an SPH formulation to one-dimensional problems only [6]. We use the 3D formulation presented by Cleary and Das [18] that uses an effective tensile strain from Melosh et al. [74] to give  $\varepsilon$  in (15):

$$\varepsilon = \sigma_{max} / \left( K + \frac{4}{3} G \right) \tag{21}$$

where  $\sigma_{max}$  is the maximum principal stress.

Damage only evolves when  $\varepsilon$  is larger than a threshold strain,  $\varepsilon_{th}$ , which, from Melosh et al. [74], is given by:

$$\varepsilon_{th} = \left( \frac{m_a k}{\rho_a} \right)^{-1/m} \tag{22}$$

### SPH solid boundary conditions

Solid boundaries are represented by triangular surface meshes. The nodes of the boundary mesh are represented in the SPH method as particles with a penalty

force applied in the normal direction using a Lennard-Jones style form based on the orthogonal distance of the moving SPH particles from the solid surface [76]. The penalty force replaces the pressure force terms in the momentum Eqs. (2) and (6) for moving–solid particle pairs. Non-slip boundary conditions in the directions tangential to the solid surfaces are applied by including the fluid–solid SPH particle pairs in the summations for the viscous stress in Eqs. (2) and (6). Whilst frictional forces between food and teeth should have little effect on breakdown behaviour in the scenarios considered here, it is worth noting that frictional forces between elastic bodies and solid surfaces have not yet been implemented, but may be the subject of future work. The orientation of normal/tangential force components is defined by the normal attached to each boundary particle. This is a flexible boundary implementation that allows very complex solid boundaries [22, 23], moving boundaries [24] and deforming boundaries [26] to be modelled. For deforming bodies, the nodal positions and the normal vectors are updated at each time step to reflect the current shape of the surface.

### Validations of SPH calculations

#### Validations of the SPH method

SPH has been shown to produce valid predictions for a large range of complicated behaviours of fluids and solids undergoing processes similar to those considered in the present study. Saliva experiences complicated free-surface flow, which has been shown to be predicted accurately by detailed comparison of free-surface shape to experimental results [28, 50, 91]. Likewise, the accuracy of calculations of complicated fluid behaviour in complex geometries [22], liquid sloshing [90, 91], particulate motion coupled to fluid flow [85, 86] and fluid mixing [88] has been verified by comparison of fluid behaviour with experimental measurements. Other processes validated by comparison with experiment and/or grid methods include interfacial flows [27] and multiphase flows [34]. Fluid–structure interactions have been studied in significant detail [28, 29, 80], and the fluid flow behaviour and calculated structural forces were found to be in excellent agreement with experimental measurements. Each of these physical processes is required in a model to adequately resolve saliva transport and mixing in the oral cavity. Solid foods are compressed, cut and fractured. Validations of the SPH method for these processes include comparison against FEM solutions for uniaxial compression of elastic solids [33], fracturing behaviour of brittle elastic solids by comparison with experiment [32] and machine cutting of metals [69].

### Validations of our SPH code

It is not sufficient to rely on general validation of the SPH method. Additionally, it is necessary to validate the specific code implementation used. The implementation used in this study has been validated for simulations of both liquids and elastic/elastobrittle solids. Cummins et al. [29] compared the experimentally measured force experienced by a rectangular column during impact in a 3D dam break scenario to predictions by the SPH code. Predictions of force and impulse on the column matched experimental results very closely. The model was found to be robust, and accuracy was found to be relatively independent from kernel complexity. Free-surface behaviour of water and interactions with complicated shapes have been shown to be predicted with high accuracy [22, 50] and with greater correlation with experimental results than with grid-based methods [50]. Sloshing of fluids has also been positively compared against experimental measurements [90]. Likewise, mixing of different fluids and interaction with moving geometries in an industrial mixer showed excellent agreement with experiments [88]. The results of these studies confirm the ability of this SPH code to predict complicated fluid flows, involving free surfaces and mixing as needed for predicting transport of saliva in the oral cavity during mastication.

Solid foods are compressed and broken down during mastication, and these processes pose difficult modelling challenges. During the first chewing cycle, food is compressed in a manner similar in nature to uniaxial compression. Das and Cleary [33] compared stress wave attributes calculated by the SPH code to those calculated using a commercial finite-element (FE) code for uniaxial compression of an elastic object. The SPH solution was found to agree very well with analytical and FE model solutions. SPH was shown to be stable and robust for elastodynamic applications, predicting a smoother response than the FE code in the early stages of loading.

Once food is sufficiently compressed, then fracturing may occur, so accurate prediction of elastic–brittle fracture is also needed for modelling of mastication. Das and Cleary [32] compared the predicted fracture behaviour of a dam under earthquake loading using SPH to the actual failure behaviour of a scale model experiment and to finite-element predictions. The crack initiation and propagation was found to accurately match the actual failure conditions of the dam. Comparisons with FE simulations of the same scenario showed good agreement; however, the SPH solution did not require foreknowledge of crack propagation zones for mesh refinement or expensive remeshing iterations, which were required for the FE model.

### Computational model of the mouth

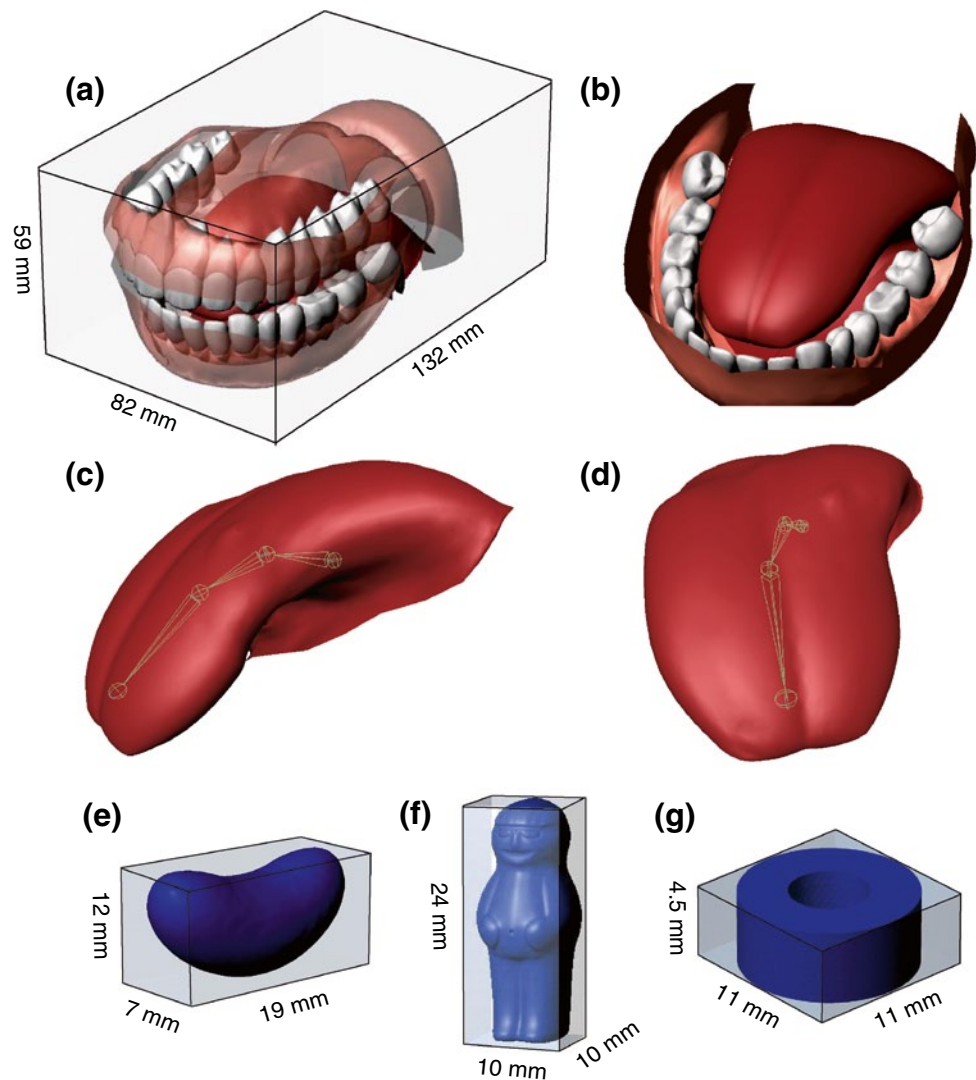
Figure 1 shows the generic geometry of the mouth used in the simulations, which includes the gums, teeth, tongue and internal cheek walls. Each of these geometries except the tongue (see below) was considered to be a non-deformable boundary. This treatment is sufficient for primary breakdown of food, as presented in this study, but compliance must be included for soft tissue structures in latter-stage chewing and swallowing. The upper jaw was fixed in place, and realistic lower jaw motion was specified for each of its six degrees of freedom (DOF). The axis of rotation of the jaw (about the temporomandibular joint) was visually identified from the 3D geometries.

The boundary nodes, which are represented as SPH particles, and boundary normals are repositioned at every time step as a result of the rigid-body motion and deformation of the boundary. In the case of liquids interacting with the tongue, teeth, gums and mouth, it is appropriate to represent the anatomical structures as rigid surfaces, with specified motions. The deformation of the tongue (described below) is not significantly affected by the resistance of the fluid. This is because the compliance of these structures is much smaller than that of the fluid. Likewise, during biting and chewing of soft foods, it is reasonable to model the teeth as moving rigid objects as any small deformation of the teeth may be too small to affect the food behaviour. The forces and torques resulting from their mechanical interaction with food were resolved at the joint centre of the jaw and are part of the predictive outputs of the model. Work done by the teeth was calculated as the dot product of the occlusal force and the displacement of a node on the teeth central to the teeth–food contact.

Realistic motion and complex deformation of the tongue were also modelled. When the tongue flexes, extends or curls, a smooth representation of its external surface is determined. This surface can dynamically interact with fluids or solids if contact is made. The tongue's external surface was generated using the linear-blending skinning functions of the commercial animation package Maya [4]. Movement of the tongue by its muscles was modelled using four spherical joints that were positioned along the length of the tongue (Fig. 1, panels c and d). The tongue surface geometry was rigged to the “virtual skeleton” made up of these joints. At any time, the position of each vertex on the surface mesh representing the tongue was determined using a weighted distribution of the rigid-body transformation resulting from rotational displacement of each joint.

Three-dimensional model representations of the food shapes (a jelly bean, a jelly baby and a hoop-shaped candy) were scaled and positioned appropriately with respect to the mouth anatomy for the beginning of the simulation.

**Fig. 1** Geometry of the model of the human oral cavity: **a** entire model, **b** lower jaw including the tongue, **c** side view of the rigged tongue and its underlying “skeleton” (joints specified by green spheres, “bones” designated by *pyramids*) rotated to the subject’s left, **d** front view of the rigged tongue and its underlying skeleton rotated to the subject’s left. The bones of the jaw, the maxilla and mandible are not included in the current model. The dimensions of the model foodstuffs considered: a jelly bean (**e**), a jelly baby (**f**) and a hoop-shaped candy (**g**) are shown



SPH particles were fitted inside a computer-aided design (CAD) surface model of each food, at a uniform spacing, on a cubic lattice that was aligned with the global axes. Whilst material properties (described below) were homogeneous in this application, individual SPH particles can be specified with individual material properties (e.g. elastic moduli or yield stress), which will be conserved as the particle displaces under load.

The material properties of solid food and saliva/liquid food during oral digestion are based on literature values where available and estimated based on similar materials where not available. Material properties are varied to study the effect of material properties on simulation results and to ensure that the modelling framework is viable for a large range of material parameters. Saliva/liquid food was represented as a Newtonian fluid with a density of  $1 \text{ g/cm}^3$  and a viscosity of  $0.01 \text{ Pa s}$  (representing the higher shear rate behaviour of normal saliva, [87]). The food material properties were based on measured properties of similar

foods (e.g. [61]). An isotropic, homogeneous, linear elastic response was assumed, which is typical in food rheological studies [1, 103] and serves as a good approximation of small-strain behaviour. The model jelly bean (Fig. 1e) was assumed to be highly ductile and had a bulk modulus of  $3.15 \text{ MPa}$ , a shear modulus of  $1.17 \text{ MPa}$  and yield stress of  $55.2 \text{ kPa}$ , with no work hardening. The model jelly baby (Fig. 1f) was assumed to be more elastic (though softer) than the jelly bean and had a bulk modulus of  $700 \text{ kPa}$ , a shear modulus of  $260 \text{ kPa}$  and a yield stress of  $55.2 \text{ kPa}$ , with no work hardening. The bulk and shear moduli of each foodstuff were also varied (by 50 % and 133 % for the jelly bean and by 50 % and 200 % for the jelly baby) to represent the uncertainty in the precise values and to study their influence on the final deformed shape and the occlusal forces during biting and chewing. The brittle candy (Fig. 1g) was assumed to have a purely elastobrittle response (negligible plastic yielding before fracture). It had a bulk modulus of  $12.5 \text{ MPa}$ , a shear modulus of  $5.8 \text{ MPa}$ ,  $k = 1 \times 10^{26} \text{ m}^{-3}$ ,

$m = 9$  and  $C_g = 45$  m/s. The flaw density,  $k$ , was scaled by factors of  $10^{-2}$  and  $10^{-4}$  to determine its effect on the nature of fracture and the loading of the teeth.

### Fluid motion in the anterior oral cavity

Saliva and liquid food can interact with hard and soft features of the oral cavity, often when the anatomical features are deforming and moving at high speed. Interactions with moving and deforming boundaries of such geometric complexity are not well handled by traditional mesh methods. As in vivo measurements of fluid velocities during interactions with these anatomical structures are not yet available, detailed quantitative validation is not yet possible. As a first step in modelling detailed saliva and liquid food flow, we qualitatively investigate the behaviour of fluid, as predicted by SPH, when interacting with the anatomy of the inferior oral cavity and the moving tongue.

### Method

The first application of the model described involves the flow of saliva or liquid food that is induced by interaction with the moving tongue. The mouth orientation is for a person in a standing position. The anterior portion was filled with fluid up to the base of the tongue. The mouth is that of a male adult with dimensions shown in Fig. 1. The fluid was represented by 343,800 particles with a spatial resolution of 0.3 mm, resulting in a volume of approximately 9 mL. Figure 2 shows the motion of the fluid over a period of 1.6 s. The deformation of the tongue that drives the fluid motion is identifiable by its changing pose in each frame. Figure 2a shows the starting position of the tongue above the fluid surface. The liquid was settled under gravity prior to modelling the action of the deforming tongue. Initially, the fluid is shown as a uniform colour so that structure of the fluid surface is visible. The conformation of the fluid to the shape of the gums and teeth at the front of the mouth can be seen. Simulations were run for 24 h (wall-clock) on six cores of a Xeon E5-2650 (Intel, Santa Clara, CA, USA).

### Results and discussion

Figure 2b shows the tip of the tongue contacting the fluid on the left side of the front of the mouth. The fluid is coloured by fluid speed, with red being the highest speeds of 0.02 m/s. Substantial velocities are seen under the tongue as the fluid is displaced by the descending tongue surface. Large ripples of fluid are visible as they travel away from the descended tongue tip. In Fig. 2c, the tongue tip has moved half of the maximum prescribed distance to the right. The fluid under the tongue is again significantly displaced, but is now moving

with a higher velocity due to the mediolateral movement of the tongue. High surface velocities are observed, especially between the tongue and the right front molars. In Fig. 2d the tongue has stopped at the extreme right position and the fluid velocities under the tongue have declined markedly. However, moderate velocities are seen to the right of the tongue as a ripple of fluid continues to travel towards the teeth on the right side of the mouth. Figure 2e shows the tongue at the same position to Fig. 2b. The surface of the fluid is less disturbed away from the tongue tip, and velocities are much lower because transients from the tongue entry have dissipated. Again, moderate velocities are seen ahead of the tongue, between its tip and the left premolars. Figure 2f and g shows the tongue as it moves further into the fluid in the extreme right and left positions, respectively. In both cases, the fluid under the tongue and ahead of the tongue displays moderate velocities, but magnitudes have decreased due to further dissipation of initial transients. The final action of the tongue is to rise out of the fluid. Figure 2h shows its position after it has risen above the surface of the fluid. Most of the surface of the fluid has flattened, but the forward action of the lifting tongue stirs the fluid in an anterior direction and generates a final large ripple with high velocities near the left incisors.

This simple application qualitatively establishes that the combined SPH–biomechanical model is suited to modelling the dynamics of fluid flow within the oral cavity. The model is capable of resolving the contact between the saliva/liquid food and the tongue, mouth and throat surfaces, even when these surfaces change in shape over time. Further work may include comparison of fluid behaviour with experimental data, variations in fluid rheology (from water to viscous foods such as yogurt) and a particle resolution study. Other important processes such as swallowing can be similarly modelled by adding appropriate biomechanical control of the other surfaces of the oral cavity such as the soft palate. Introduction of fluid particles at specific areas of the oral cavity surface is straightforward and can naturally model the secretion of saliva. Compositional change of food materials from solids to paste can also be modelled as finely chewed food is mixed with saliva or liquid food. Chemical interactions between fluids and foodstuffs can also be studied. The inclusion of diffusion equations for chemical reaction and chemical digestion coupled to the fluid flow has already been developed for SPH [24, 25] and could be used to model the dissolution and transport of flavour components.

### Biting of an elastoplastic foodstuff by the incisor teeth

#### Method

The second application demonstrates the ability of a coupled SPH–elastoplastic–biomechanical model to predict



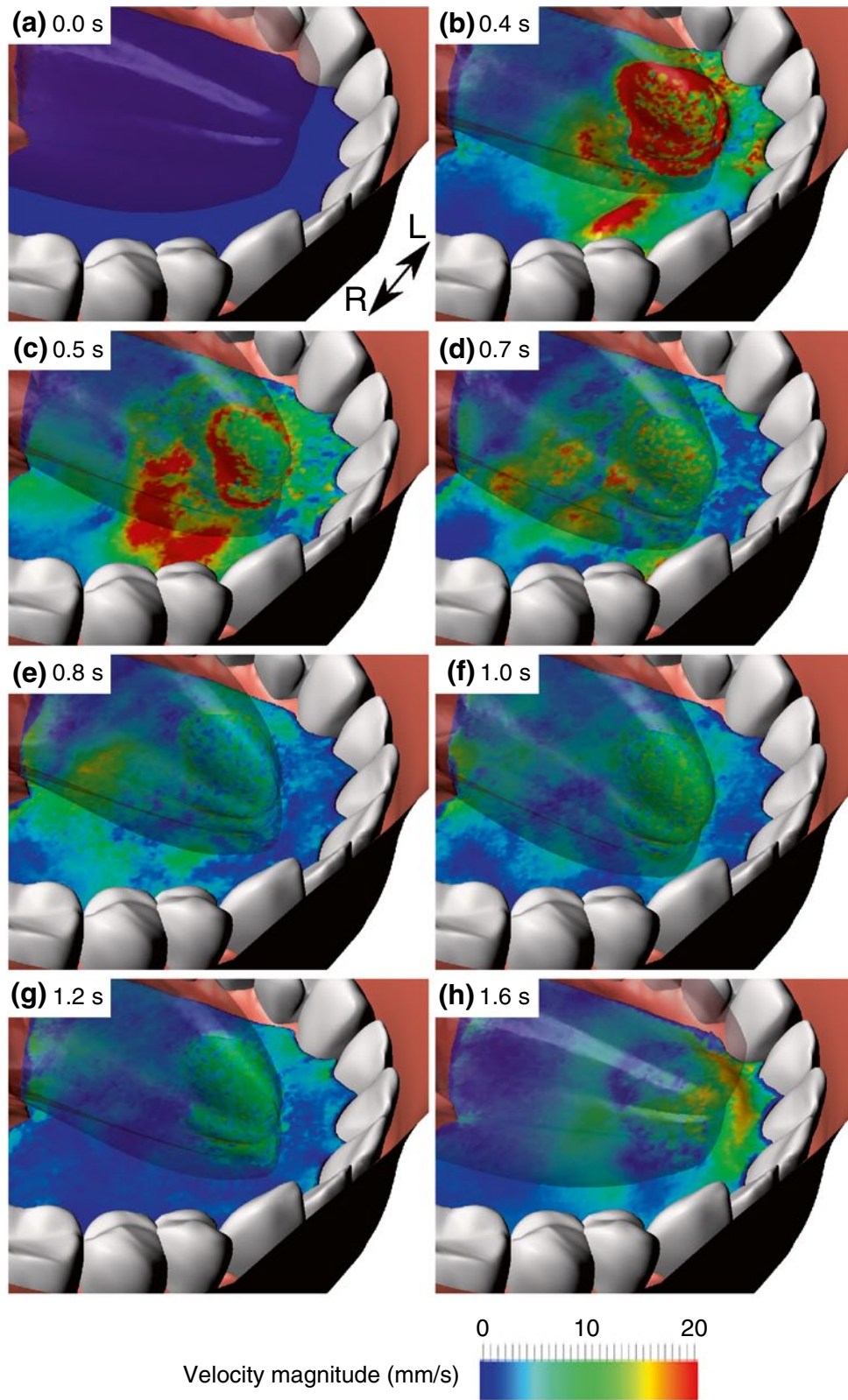


**Fig. 2** Fluid motion in the anterior oral cavity induced by tongue movement and inertial forces. The tongue is made transparent to allow the fluid flow under the tongue to be seen. **a** Shows the starting position of the tongue, which is above the flowing fluid. Left (L) and

right (R) directions are defined. **b–f** Show the tip of the tongue contacting the saliva and then moving left to right and back. The fluid is coloured by velocity magnitude

primary cutting of a foodstuff by the incisors. Ingestion of solid food often requires cutting by biting to reduce food to a size that suits chewing. A model jelly bean is used as an example elastoplastic solid. It was placed between the top and bottom middle incisor teeth on the right side of the mouth. The dimensions of the mouth and jelly bean are shown in Fig. 1 (panels a and e). The jelly bean was represented by 28,000 SPH particles with a spacing of 0.24 mm. A particle resolution study confirmed insensitivity of occlusal force results at this resolution or higher (within an error margin of 4 %). Three variations in elastic moduli were considered. The bulk moduli,  $K$ , of the least stiff, intermediate and stiffest beans were 2.1, 3.15 and 4.20 MPa, respectively. The shear modulus,  $G$ , was set as a constant proportion of  $K$  ( $G = 6/13 K$ ), which corresponds to a Poisson's ratio of 0.3. Whilst a jelly bean may display some nonlinearity in its elastic response, a linear elastic material model serves as a good first approximation of the actual material behaviour. Material isotropy was assumed due to the lack of fibrous structures (such as in carrots) or other sources of anisotropy. Biting was simulated by purely rotational motion of the lower jaw in the sagittal plane from an open position to a position when the incisors make contact; specifically, the jaw was rotated 8 degrees about jaw joint axis in the sagittal plane over a period of 0.8 s. Simulations were run for 450 h (wall-clock) on eight cores of a Xeon E5-2650 (Intel, Santa Clara, CA, USA).

## Results and discussion

Figure 3 shows the changes in physical shape, von Mises stress and plastic strain of the jelly bean during the biting process. After 0.2 s, compressive stress has developed in the parts of the bean close to the top and bottom incisors. The teeth have already cut the bean to a small degree. However, deformation and plastic strain of the bean are negligible away from the contact areas with the teeth. At 0.45 s, more of the bean has been cut by direct penetration of the teeth surfaces. The von Mises stress in the part of the bean between the teeth has risen to the material yield stress. This leads to significant deformation and plastic strain, which remains localised to the volume of the bean close to, and directly between, the teeth contact surfaces. At 0.7 s, the jelly bean has been split apart by the teeth. The stresses are similar to those at 0.45 s, but plastic strain is now greater than unity over the entire cut surface. The strain levels around the cutting surfaces of the incisors are very high, and significant topological change in the structure of the foodstuff occurs as the material between the teeth is forced plastically out of the way of the approaching teeth. These features, combined with the moving complex-shaped surfaces of both teeth and foodstuff, make this scenario exceedingly difficult to simulate with FE methods. However, with SPH

operating in a Lagrangian frame, all the relative movements have no impact on the calculation and the very high deformations are handled easily by the meshless formulation.

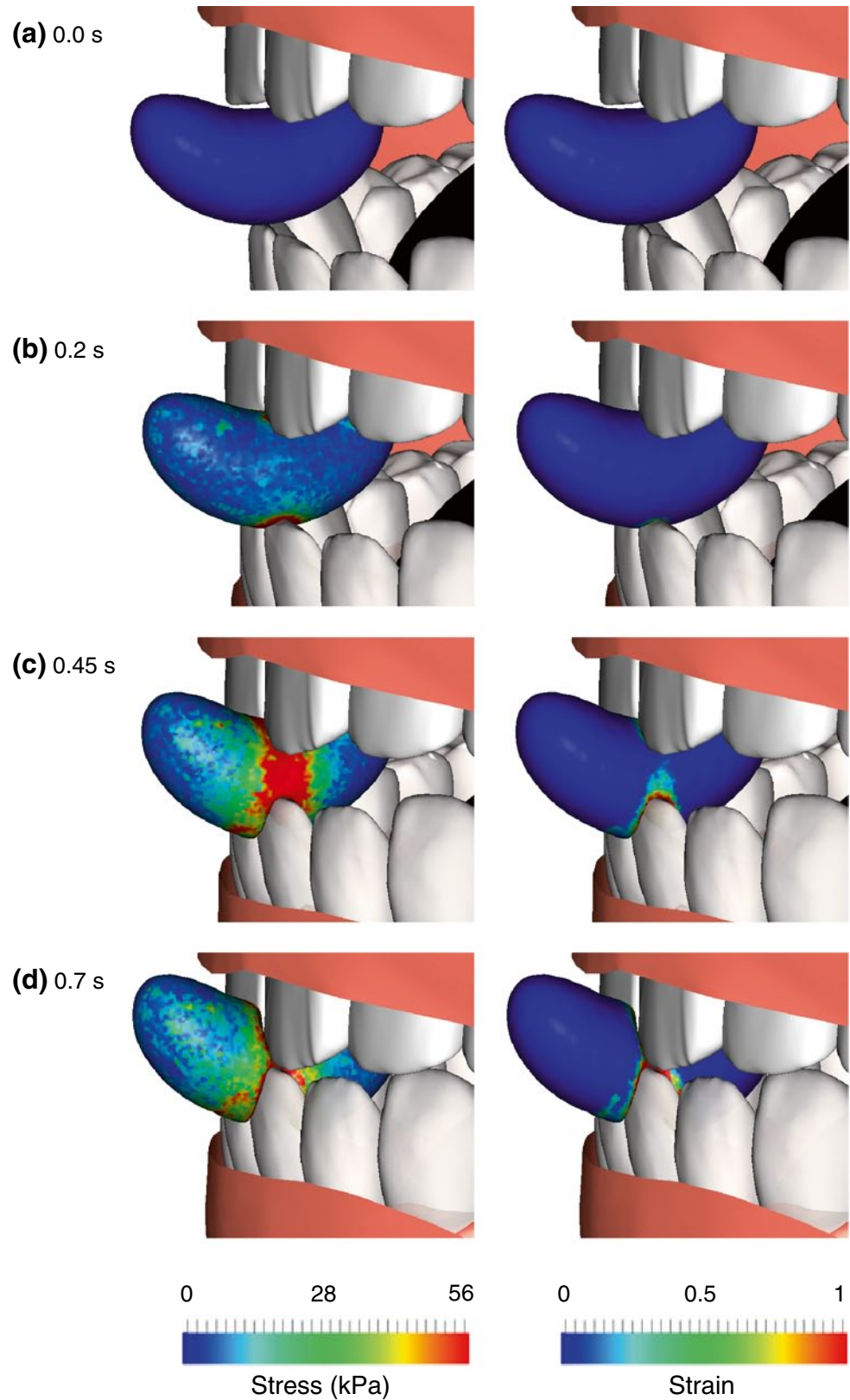
Figure 4 shows the variation in the vertical component of occlusal force with variations in the elastic moduli (bulk and shear) of the jelly bean. It also shows the shape of the jelly bean, coloured by von Mises stress, for each of the three variations in elastic moduli at three different times in the cutting simulation. The magnitude of force predicted is similar to cutting measurements for a somewhat similarly soft food (a raisin [103]) and within controllable movement by the jaw [58]. It is worth noting that the force results are small compared to the force generated by more than one pair of teeth during maximal biting [99]. Biting of a jelly bean requires much less than the maximal force that is typically measured experimentally.

Whilst direct comparisons with an experiment are not currently available for such a material, the force traces in Fig. 4 show characteristic features seen in experimental biting measurements of other foods [60, 61, 105], specifically

1. An early peak (near 0.1 s) during which initial yielding of the bean occurs near the teeth;
2. A steep rise in applied force;
3. A second, much higher peak at approximately 0.38 s, which is the maximum force of biting; and
4. A steady decrease in force until the foodstuff is bitten into discrete pieces.

Features of the deformed shape of the beans and the distributions of von Mises stress shown in Fig. 4 can be correlated with the timing of the two peaks, marked A and B. Before yielding occurs, the contact surfaces between the teeth and bean are convex and non-conforming so surface stresses rise quickly. Row A of Fig. 4 shows that the deformation of the beans is not visible at the time of the first peak A and that high stresses have developed only at the points of contact between the jelly bean and teeth where the stress is equal to the yield stress. The yield stress places an upper limit on stress (see the maximum stress column in Table 1), and so the force required to compress yielded material also has an upper limit. Further applied load generates plastic flow of the material to either side of the approaching teeth and begins the cutting action of the incisors. As material flows to the sides, there is less present between the teeth to resist their approach. This geometric softening (as described by [9]) of the bean reduces the load transmitted to the teeth. After initial yielding, the occlusal force rises again. The bean material now better conforms to the shape of the teeth due to the cutting action. Surface stresses reduce, and less geometric softening occurs until the timing of the second peak. Row B of Fig. 4

**Fig. 3** Cutting of an elastoplastic solid jelly bean during biting by the incisors. The jelly bean is coloured by the Von Mises stress in the left panels and by plastic strain in the right panels



shows that the bean material between the top and bottom incisors experiences fairly uniform compressive stress equal to the yield stress at the time of the second peak

(marked as B on the force plot in Fig. 4). Larger-scale plastic flow of bean material is now possible. Significant cutting of the jelly bean by the incisors occurs after the

**Fig. 4** Variation in the vertical component of occlusal force and the deformed shape of the jelly bean for different bulk moduli ( $K$ ) of the bean. Its shape coloured by the von Mises stress is displayed at three times of the biting simulation, denoted by the letters *A*, *B* and *C*. The times for which these deformed shapes occur are indicated by the same letters on the force–time graph

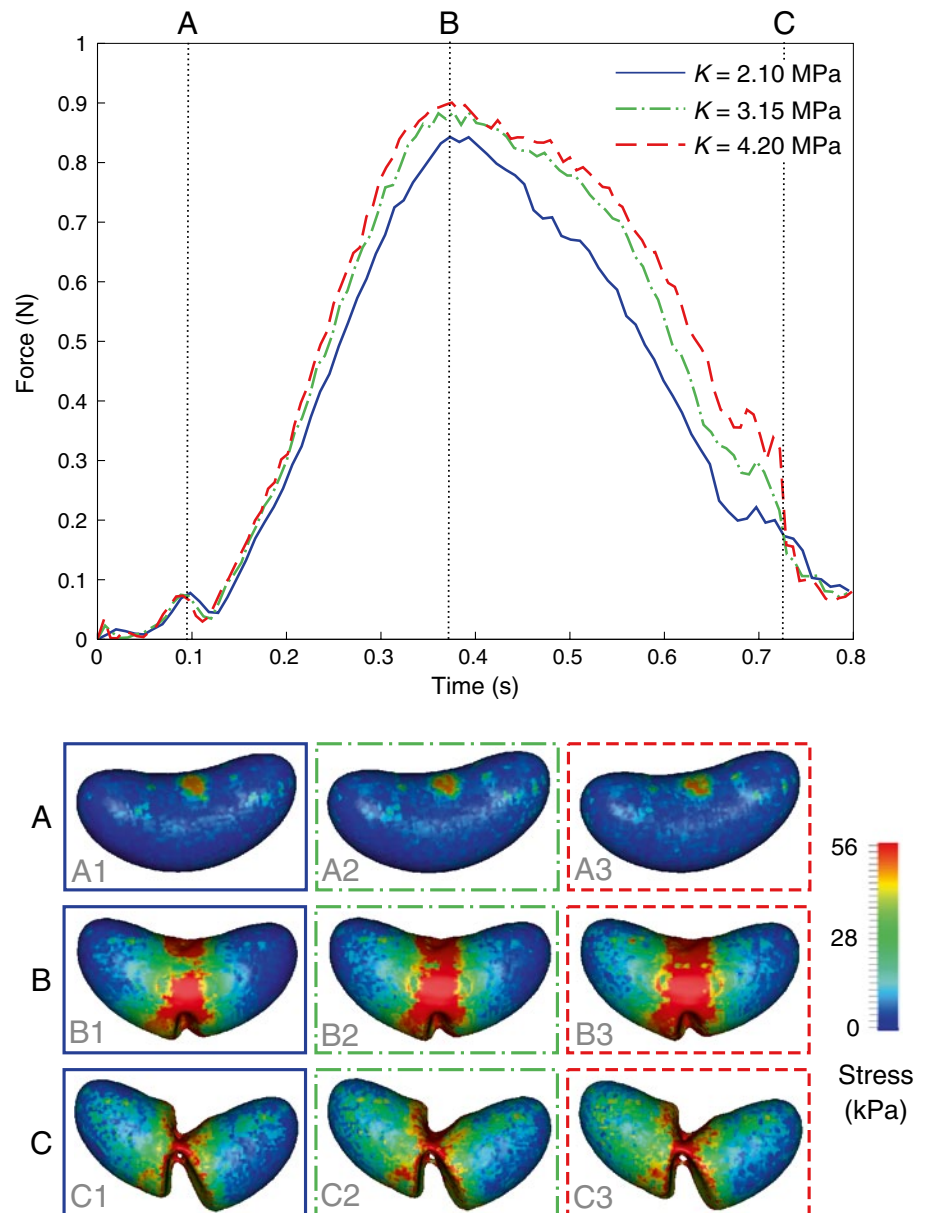


**Table 1** Spatially averaged (mean) and maximum von Mises stress and plastic strain in the jelly beans during biting by the incisors at 0.8 s of simulation time

Young's modulus (MPa)	Von Mises Stress (kPa)		Plastic strain	
	Mean	Maximum	Mean	Maximum
2.10	24	55	0.11	6.3
3.15	23	55	0.12	7.0
4.20	25	55	0.13	8.5

second peak in the occlusal force. Row *C* of Fig. 4 shows the shape of the jelly beans after the teeth have nearly cut the bean into two disjoint pieces. Very little material remains between the teeth to resist their approach and

so the occlusal force declines from the second peak to approximately zero.

The loading on the teeth and the stresses in the beans were only modestly dependent on the elastic material properties of the bean. Whilst  $K$  varies by  $-50$  and  $+33$  %, from that of the intermediate material, the peak force varies by less than 4 % (top panel of Fig. 4). Similarly, the final mean stress also varies by less than 5 % (as shown in Table 1). The stress distribution within the bean, shown in rows *A*, *B* and *C* of Fig. 4, is also very similar. Before yielding occurs, the beans resist penetration by the teeth, transmitting load in proportion to the elastic stiffness. So, the peak occlusal load is largest for the stiffest bean. The occlusal load and the stresses in the beans vary little with elastic moduli because:

**Table 2** Spatially averaged (mean) and maximum von Mises stress and plastic strain in the central 0.8-mm longitudinal section of the jelly beans during biting by the incisors at 0.8 s of simulation time

Young's modulus (MPa)	Von Mises stress (kPa)		Plastic strain	
	Mean	Maximum	Mean	Maximum
2.10	34	55	0.31	6.3
3.15	33	55	0.34	7.0
4.20	35	55	0.35	8.6

1. the yield stress was the same for each material, and in each case it was small in proportion to bulk modulus (i.e. jelly beans are very plastic); and
2. the high (knifelike) aspect ratio of the incisor–bean contact areas produced large local stresses, which quickly induced local yielding of bean material, meaning that the mechanical response is predominantly plastic in nature.

Small differences in the timing of the two peaks of occlusal force were also produced by changes in the bean moduli. Stress rises more quickly in the stiffest bean for the same level of strain leading to earlier yielding. The von Mises stress is therefore highest for the stiffest bean and lowest for the least stiff bean at the timing of the first and second peaks (see the jelly bean shapes A and B in Fig. 4). The two peaks of force occur first for the stiffest jelly bean and last for the softest bean. The spatially averaged and maximum magnitudes of stress and plastic strain in the bean at 0.8 s are listed in Table 1. The final von Mises stresses are similar for each of the three moduli (see row C in Fig. 4), but the spatially averaged and maximum plastic strain at the end of the cutting process is markedly higher for larger elastic moduli. Table 2 shows the peak and spatially averaged results of plastic strain and von Mises stress for the 8-mm-long central region of the jelly bean, where deformation by the teeth is greatest. The maximum von Mises stress and plastic strain values in Table 2 are identical to those in Table 1. The mean von Mises stress is again similar for each of the three elastic moduli but more than 40 % larger than the average over the entire sample. The mean plastic strain is also similar for each of the three elastic moduli, but more than 170 % larger than the average over the entire jelly bean.

The occlusal loading is more highly dependent on the yield stress ( $Y$ ) of the bean than the elastic moduli. Figure 5 shows the variation in the vertical component of occlusal force with variations in  $Y$ . It also shows the shape of the jelly bean, coloured by von Mises stress, for each of the three variations in  $Y$  at three different times in the cutting process. At approximately 0.05 s, the force trace rises linearly until initial yielding occurs at the surface of the bean.

As in Fig. 4, the force peaks as initial yielding occurs, and the peak force increases with increasing  $Y$ . Row A of Fig. 5 shows that the shape of the jelly bean is similar for the three variants of  $Y$ , but the stress in the deformed volume (at the tooth–bean contact surface) increases with  $Y$ . After initial yielding, the force decreases, to a greater degree with increasing  $Y$ . For the largest  $Y$  case, the force decreases to zero, but for lower  $Y$ , it decreases to a lesser extent and remains positive. After 0.1 s, the force increases approximately linearly, with gradient increasing with  $Y$ . The occlusal force peaks at approximately 0.34 s for all cases of  $Y$ , and the magnitude of peak force increases linearly with  $Y$  (with a correlation coefficient,  $R^2 = 1.00$ ). As described previously, the occlusal force peaks when the volume of jelly bean material between the teeth has yielded (see row B of Fig. 5). Row B of Fig. 5 shows the impression of the lower incisor in the jelly bean due to plastic flow after initial yielding. Larger-scale plastic flow occurs as the jaw closes further, and the separation of the jelly bean into two pieces is accompanied with a reduction in occlusal force (after 0.34 s, as also described for Fig. 4). As the jelly beans are separated into two fragments (row C of Fig. 5), the occlusal force drops to zero, at a faster rate with larger  $Y$ . When the jelly bean has nearly separated into two pieces (0.7 s), the bean pieces move under gravity and the force trace shows additional noise as contact between the food and teeth is lost and restored. The magnitude of stress in the volume of the beans between the approaching teeth, shown in row C of Fig. 5, increases with  $Y$ , but the final deformed shape is similar for each of the three material cases.

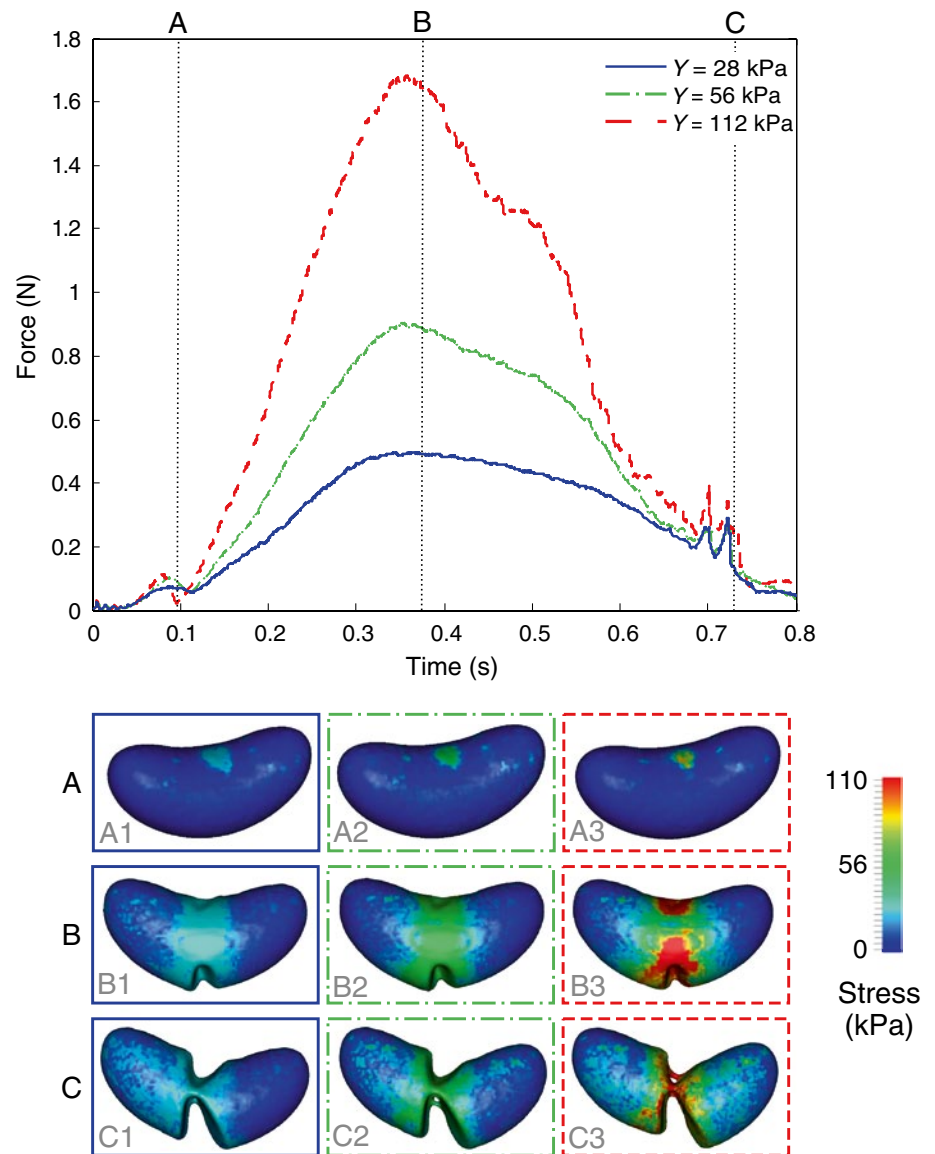
Cumulative work done by the teeth during each of the simulation cases is shown in Fig. 6. In each case, the work displays a sigmoidal shape, due to the small amounts of force exerted on the teeth in the early and latter stages and the large amount of force exerted between 0.25 and 0.60 s. Hence, the majority of work is done from 0.25 to 0.60 s. As with the plots of force (Figs. 4, 5), the work done by the teeth increases strongly with  $Y$  (with a 40 % difference between  $Y = 55$  kPa and  $Y = 110$  kPa behaviour as seen in Fig. 6b), but only varies by 13 % over a range of bulk modulus from 2.10 to 4.20 MPa (Fig. 6a). Ignoring any co-contraction in the jaw muscles, this measure of work is indicative of muscular effort and suggests that muscular effort increases only modestly with increased  $K$  and  $G$ , but increases significantly with increased  $Y$ .

## Chewing of elastoplastic food by the molars

### Method

Progressive damage due to chewing of an elastoplastic foodstuff by the molars is presented as the third

**Fig. 5** Variation in the vertical component of occlusal force and the deformed shape of the jelly bean for yield stress ( $Y$ ) of the bean. Its shape coloured by the von Mises stress is displayed at three times of the biting simulation, denoted by the letters *A*, *B* and *C*. The times for which these deformed shapes occur are indicated by the same letters on the force–time graph



application of the coupled SPH–elastoplastic–biomechanical model. After ingestion, chewing is the next important process in early digestion. Chewing serves a number of purposes; specifically, large items of food are crushed and broken into smaller portions, saliva is mixed with solid food to enable more efficient transport, flavours are released, and enzymes in the saliva begin the chemical breakdown of the food. Only the first of these processes, the mechanical breakdown of food, is presented in this study. The example elastoplastic foodstuff, a model jelly baby, was represented by 35,500 particles with a spacing of 0.3 mm. The dimensions of the mouth and jelly baby are shown in Fig. 1 (panels a and f). Consistent with measured chewing jaw kinematics [7, 67], the jaw motion was represented by periodic translations of 4 mm amplitude in the vertical direction and  $180^\circ$  out of phase translations in

both the anteroposterior direction (1.5 mm amplitude) and mediolateral directions (0.5 mm amplitude). Separate simulations were also run with the jelly baby shifted 10 mm posteriorly and 10 mm anteriorly to study the effect of starting position on occlusal force and deformed shape of the jelly baby after chewing. Interaction with the tongue was excluded in this application as its motion has not been characterised in sufficient detail for this type of modelling. However, note that repositioning of food by the tongue has been observed previously as an important component of mastication [52]. This may be considered in future development of this work. The period of one opening and closing of the jaw was 1 s, and three chewing cycles were modelled. Simulations were run for 360 h (wall-clock) on seven cores of a Xeon E5-2650 (Intel, Santa Clara, CA, USA).

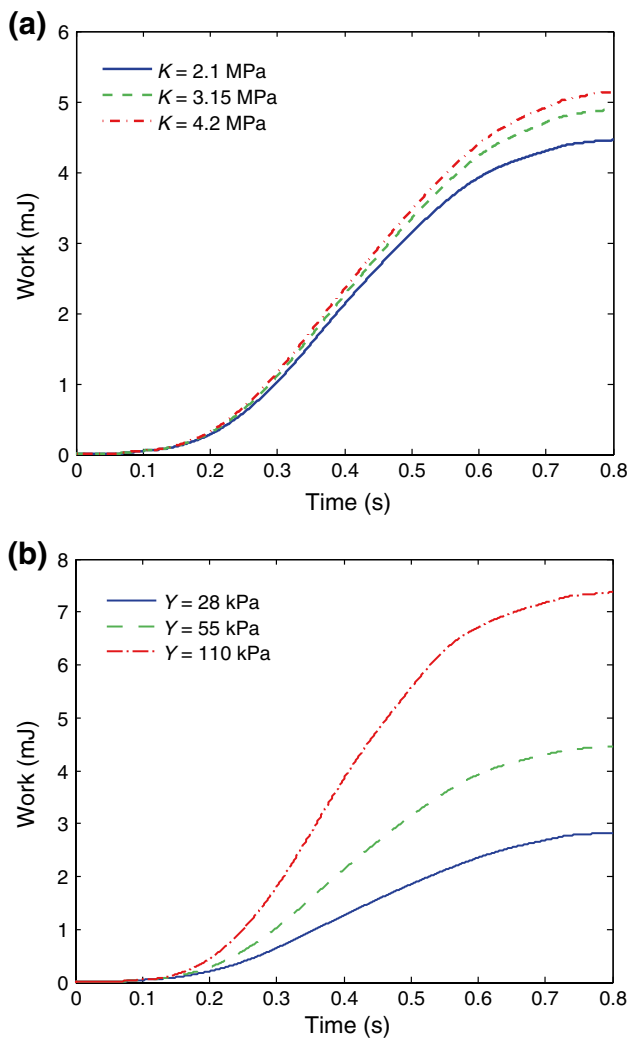


**Fig. 6** Cumulative work done during the biting of the jelly bean for **a** three variations in elastic moduli ( $K$  and  $G$ ) and **b** three variants of yield stress ( $Y$ )

## Results and discussion

Figure 7 shows the progressive squashing of the foodstuff with repetitions of the chewing action. The jelly baby initially has zero stress and strain. At 0.5 s the jaw is closed, and significant deformation of the foodstuff has occurred. Portions of the head, body and legs that were situated between the approaching teeth at the point of contact have now flowed out through gaps between the molars. The stresses in the areas of the jelly baby compressed by the teeth are high and reach the yield stress in many regions. After 1.0 s, the jaw has reopened and the top teeth are no longer in contact with the jelly baby. The jelly baby clearly retains the impressions from the top teeth. Significant plastic strain is present where the impressions of the top teeth are visible, but stresses have decreased markedly because

occlusal loading has been removed. After the second cycle of jaw closing (ending at 1.5 s), the stresses in the portions of the jelly baby compressed by the teeth are nearly identical with the stresses in the first cycle of jaw closing (at 0.5 s). Likewise, after the second and third cycles of jaw opening (ending at 2.0 and 3.0 s, respectively), the deformation, plastic strain and von Mises stress of the jelly baby are almost identical with the results at 1.0 s. In the first cycle of jaw closing, a large amount of jelly baby material flows plastically away from the teeth as the material changes to conform to the shapes of the teeth surfaces. The remaining material responds with little further yielding, but as a large amount of material no longer contacts the teeth, the occlusal force is diminished. This result demonstrates that chewing without accompanying tongue motion, which assists by repositioning the foodstuff, has little effect after the first chewing cycle. The interactions with the tongue may be characterised for future simulations and incorporated into the model.

Figure 8 shows the variations in the magnitude of the occlusal force with variations in the bulk and shear moduli of the jelly baby. The shape of the jelly baby, coloured by von Mises stress, is also shown for each of the three variations in elastic moduli at six different times in the chewing process. The occlusal force is zero for the first 0.1 s because contact has not been made between the top teeth and the jelly baby. After the top teeth make contact with the jelly baby, the force increases to a maximum, which coincides with the maximum amplitude of vertical jaw motion. Occlusal force then decreases to zero halfway through the jaw opening phase when contact is lost between the upper jaw and the foodstuff. The magnitude of the maximum force decreases in the second and third cycles of chewing. The von Mises stresses show a corresponding trend to the plots of occlusal force. They are highest at 0.5 s (see row A of Fig. 8), have declined at 1.5 s (see row B of Fig. 8) and have reduced further at 2.5 s (see row C of Fig. 8). For all three cases, the stress in the jelly baby is significantly lower when contact is lost with the upper teeth (rows B, D and F of Fig. 8) than when it is compressed by the teeth (rows A, C and E of Fig. 8).

The occlusal force, the deformed shapes of the jelly babies and the resultant stress and plastic strain depend on the elastic moduli of the foodstuff. As in the biting application, the occlusal force is larger for materials with higher bulk and shear moduli. Row F of Fig. 8 shows that the stiffer jelly baby experiences larger deformation for the same jaw motion. The von Mises stress and plastic strain of the jelly baby during jaw closure increase with increasing bulk modulus (rows A, C and E of Fig. 8). Similarly, stresses in the jelly babies after jaw opening (at 0.75, 1.75 and 2.75 s, respectively) also increase with increasing bulk modulus (rows B, D and F of Fig. 8).

**Fig. 7** Progressive squashing of a model jelly baby during chewing by molars. The jelly baby is coloured by von Mises stress in the left panels and plastic strain in the right panels

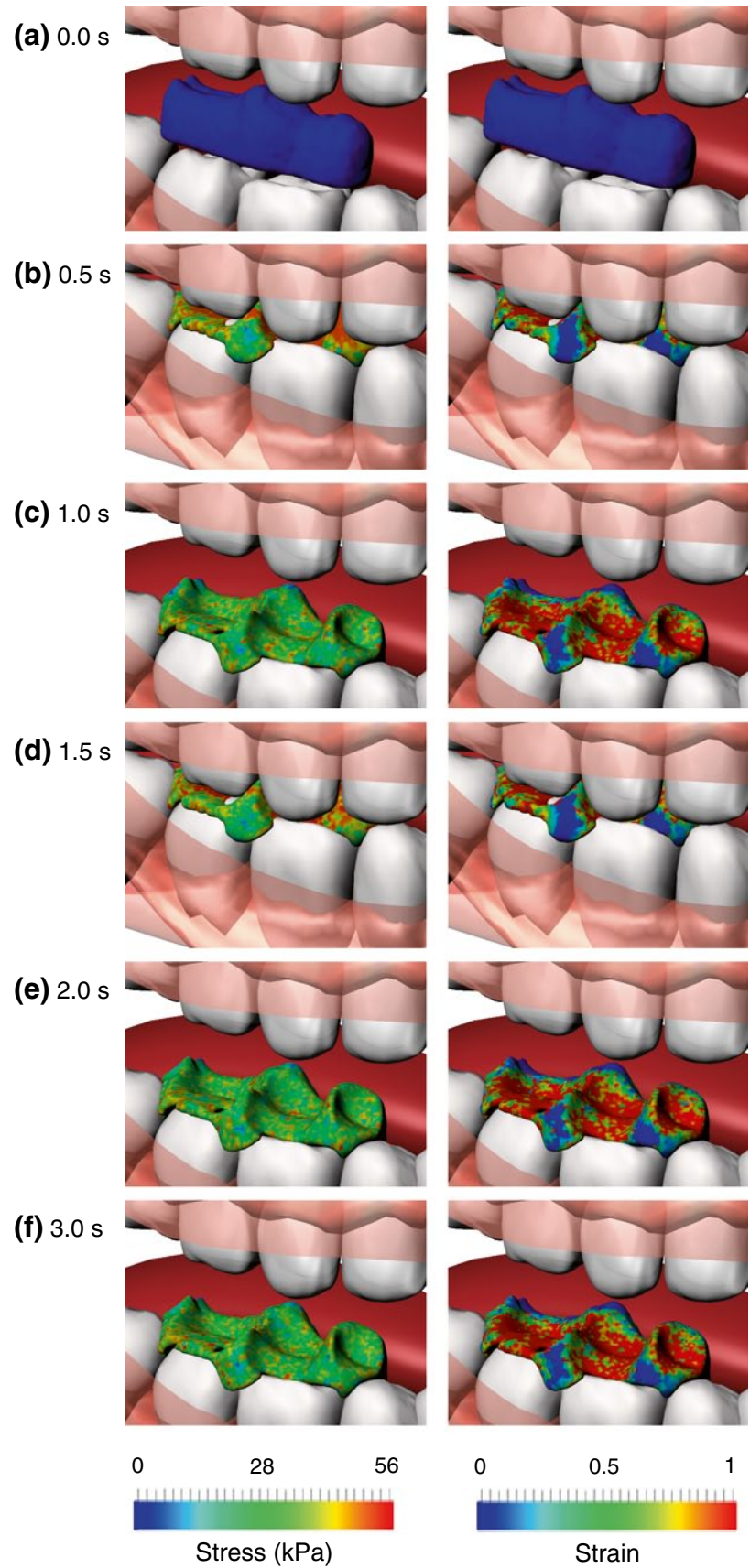
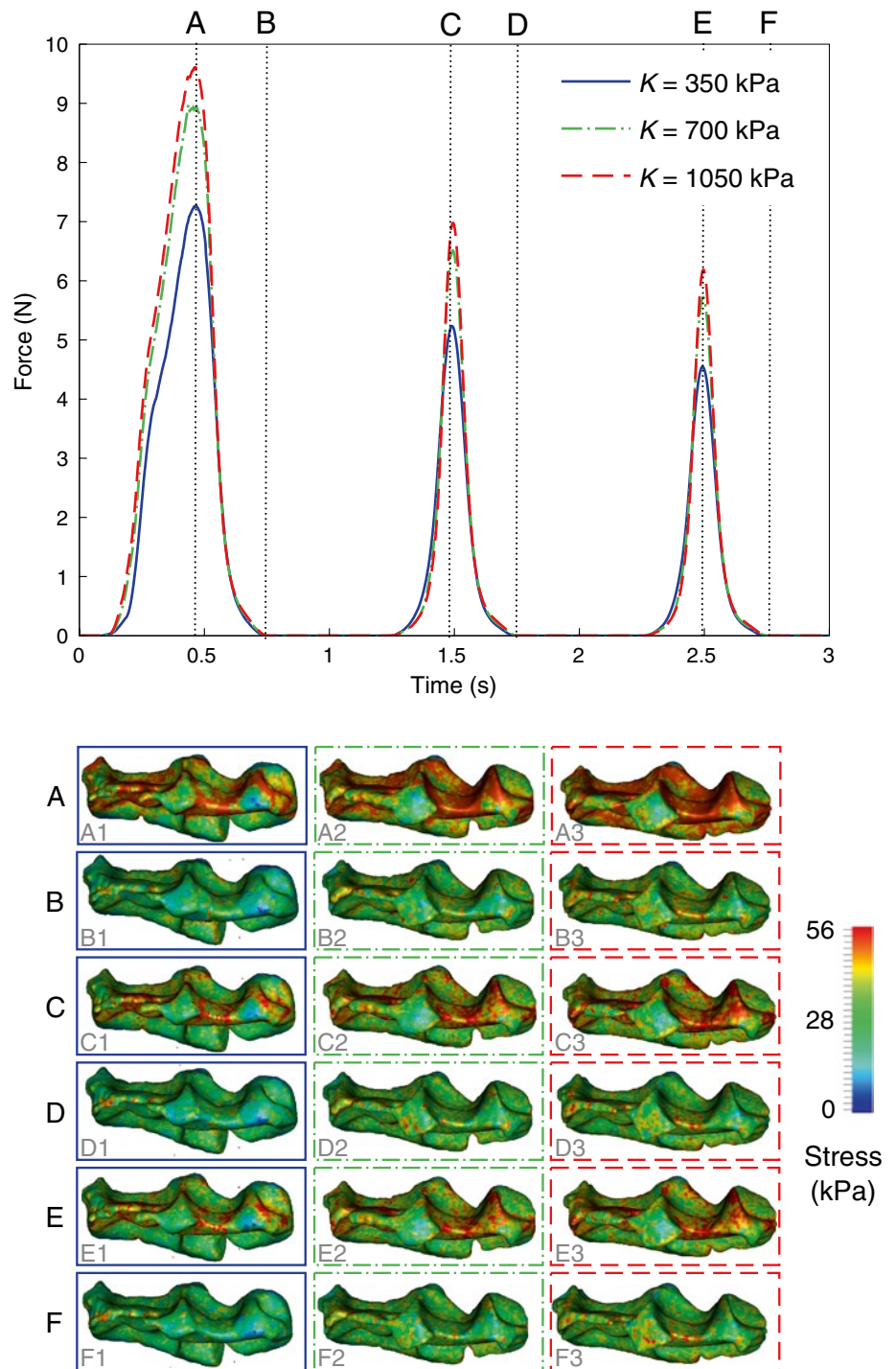




**Fig. 8** Variation in the magnitude of occlusal force and the resultant shape during chewing of the jelly baby for different bulk and shear moduli of the foodstuff. The deformed shape of the jelly baby coloured by von Mises stress is displayed at six times, denoted by the letters from A to F. The times for which these deformed shapes occur are indicated by the same letters on the force–time graph



At the timing of the first peak of force, the spatially averaged von Mises stress and mean and peak plastic strains (Table 3) all increase with increasing bulk modulus. For larger elastic moduli, the stresses rise more quickly for the same rate of applied deformation and the regions experiencing higher stress yield earlier, resulting in greater plastic flow of the material. This leads to greater deformation of the chewed foodstuff for the same jaw kinematics. The final

spatially averaged von Mises stress and mean and peak plastic strains are listed in Table 4. After the third chewing cycle, the mean stress is lower than during the first peak of force (Table 3). This is because the occlusal loading is zero and only residual stresses remain. The maximum stress has peaked at the yield stress. Peak and spatially averaged plastic strain increases from the time of the first peak (at 0.5 s, see Table 3) to the end of the third chewing cycle (at

**Table 3** Spatially averaged (mean) and maximum von Mises stress and plastic strain in the jelly babies during chewing by the molars after 0.5 s of simulation time

Young's modulus (kPa)	Von Mises stress (kPa)		Plastic strain	
	Mean	Maximum	Mean	Maximum
350	38	51	0.3	2.6
700	43	51	0.5	3.7
1050	45	51	0.6	4.1

**Table 4** Spatially averaged (mean) and maximum von Mises stress and plastic strain in the jelly babies during chewing by the molars after 3.0 s of simulation time

Young's modulus (MPa)	Von Mises stress (kPa)		Plastic strain	
	Mean	Maximum	Mean	Maximum
350	22	55	0.4	4.6
700	31	55	0.6	5.1
1050	34	55	0.7	6.1

around 3.0 s, see Table 4), but the trend of larger strains for materials with higher elastic moduli remains.

The occlusal forces predicted for the chewing simulations were approximately 10 times larger than for the biting simulation even though bulk modulus of the chewed jelly baby was 4.5 times smaller than the bitten jelly bean. This was due to the different pressure profiles applied to the foodstuffs by the knifelike surface of the incisors and the larger, flatter surfaces of the molars. The incisors produce very large contact pressures on the food because the area of contact is very small. These high pressures lead to localised yielding and plastic flow of the material close to the teeth, which is the only source of resistance to the approaching teeth. This means that the force required to yield the jelly bean is actually quite small. Conversely, the molars distribute contact force over a much larger area, leading to more of the food material yielding to the same degree. The combination of more of the material responding elastically and a much larger teeth–foodstuff contact area (at least 10 times larger) results in larger occlusal forces than for biting.

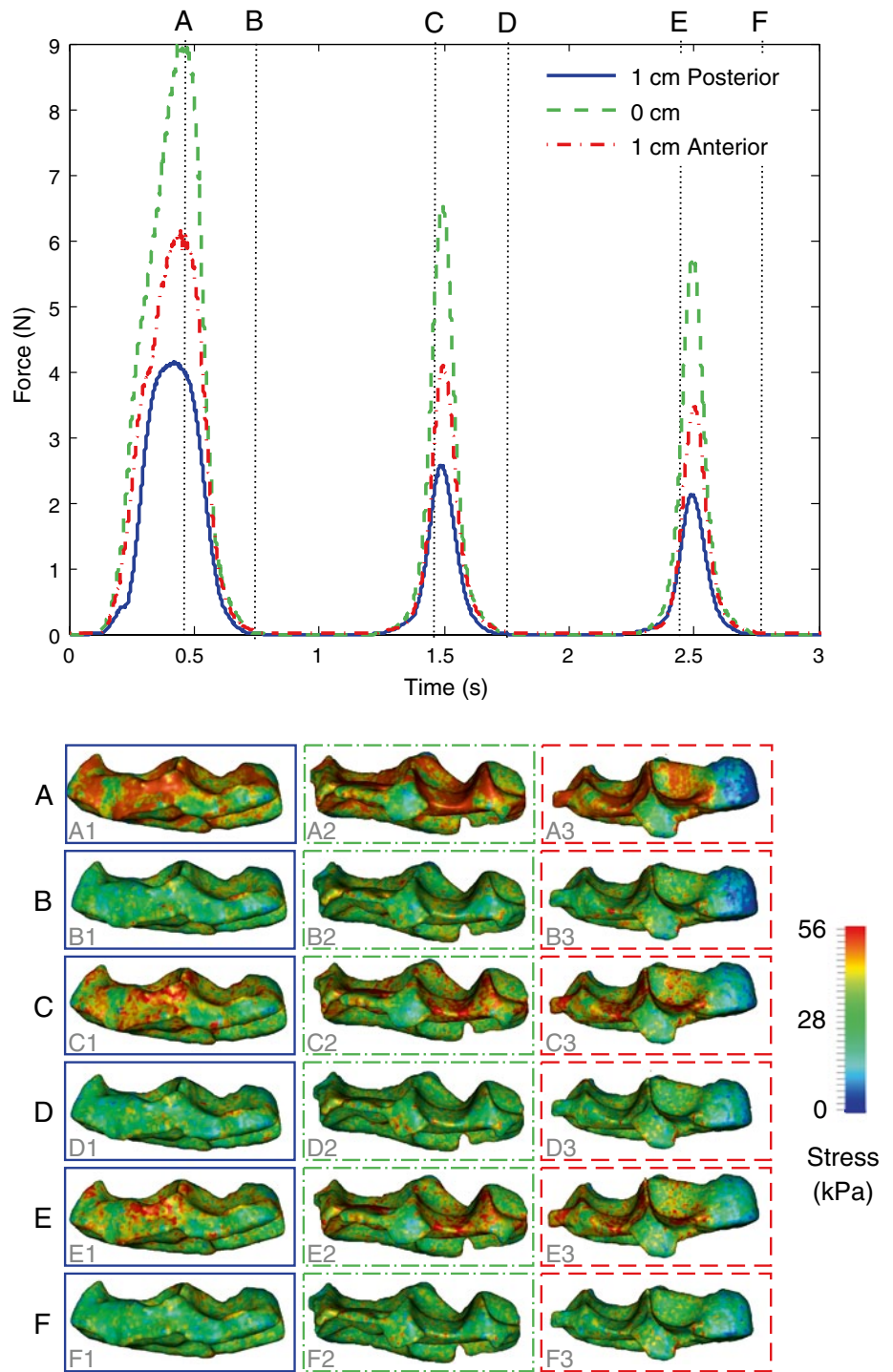
The magnitude of occlusal force and the final deformed shape are significantly dependant on the initial position of the jelly baby. Figure 9 shows the variations in the magnitude of the occlusal force with variations in initial location of the jelly baby. Again, the shape of the jelly baby, coloured by von Mises stress, is also shown for each of the three variations in initial location at six different times in the chewing process. The force traces for the 1 cm anterior and 1 cm posterior cases are of similar shape but at least 33 % and 44 % lower in magnitude than for the original position, respectively. These reductions in force are due

to less jelly baby material interacting with the teeth for the alternative initial positions. For the original case, three teeth from the top jaw make contact with the jelly baby and indent the foodstuff through the majority of its volume. The impressions of the three teeth are visible in the images of the deformed jelly baby (column A2 to F2 of Fig. 9). For the 1 cm anterior case, only two teeth from the top jaw contact the jelly baby (column A3 to F3 of Fig. 9). The teeth still indent the foodstuff through the majority of the volume of the jelly baby, but the contact area is smaller (two teeth instead of three) so the force is reduced, approximately by a factor of one-third. The forces in the 1 cm posterior case are less than for the other two cases because only two teeth from the top jaw contact the jelly baby and because the teeth only indent the foodstuff approximately halfway through its volume (column A1 to F1 of Fig. 9). Again, the contact area is smaller for the 1 cm posterior case than for the original case, but also the strain imposed on the jelly baby is lower, leading to a much smaller level of occlusal force.

The work done by the jaw during chewing of a jelly baby is shown in Fig. 10. In all cases, it increases as the first chewing cycle progresses, but plateaus at the start of the first peak of occlusal force (0.5 s). After the first chewing cycle, very little additional work is performed. This result highlights the need for relocation of the foodstuff by movement of the tongue and mandible. As most of the work is done in the first chewing cycle for this foodstuff, the second and third cycles are relatively inefficient. The work done increases with increasing elastic modulus (Fig. 10a) and is larger for the original position case than for the 1 cm anterior and 1 cm posterior cases. In reality, humans alter our jaw kinematics during chewing to suit the texture and position of foodstuffs in the oral cavity [53]. Future studies using food-specific jaw kinematics are required to understand how different foods are broken down.

A number of other model features may need to be incorporated into the model to consider the latter stages of chewing. Repositioning of food by interaction with the tongue will need to be investigated. The cheeks and tongue can also both be represented in the model as deformable objects in the same way as the tongue was represented in “Fluid motion in the anterior oral cavity”. Ideally, these deformations would be sourced from video tomography of actual chewing. Simulation of the compliance of these structures may become necessary when interacting with each other or hard foods. Occlusal force is sensitive to jaw kinematics. Jaw motions also change during chewing as the food is broken down, if muscles fatigue and jaw motions differ for foods with different breakdown behaviours [52]. Jaw motion can be measured using video motion capture techniques and implemented

**Fig. 9** Variation in the magnitude of occlusal force and the resultant shape during chewing of the jelly baby for three different initial positions of the food-stuff (shifted: 10 mm anteriorly, 0 mm and 10 mm posteriorly). The deformed shape of the jelly baby coloured by von Mises stress is displayed at six times, denoted by the letters from A to F. The times for which these deformed shapes occur are indicated by the same letters on the force–time graph



for a specific food type. Results can be validated by measuring occlusal force and comparing predicted food fragment sizes against model predictions. As saliva is mixed into the food, the changes to food fragment mechanical properties, lubrication and the agglomeration in a bolus must be modelled. Also, as flavour compounds are released, the transport of tastants and aromas to their receptors must be considered.

**Fracture of brittle food from a single bite**

**Method**

The fourth application of the model focuses on the fracture of a brittle material during biting. Unlike the foodstuffs considered in the previous two sections, brittle food fails by fracturing with little or no plastic

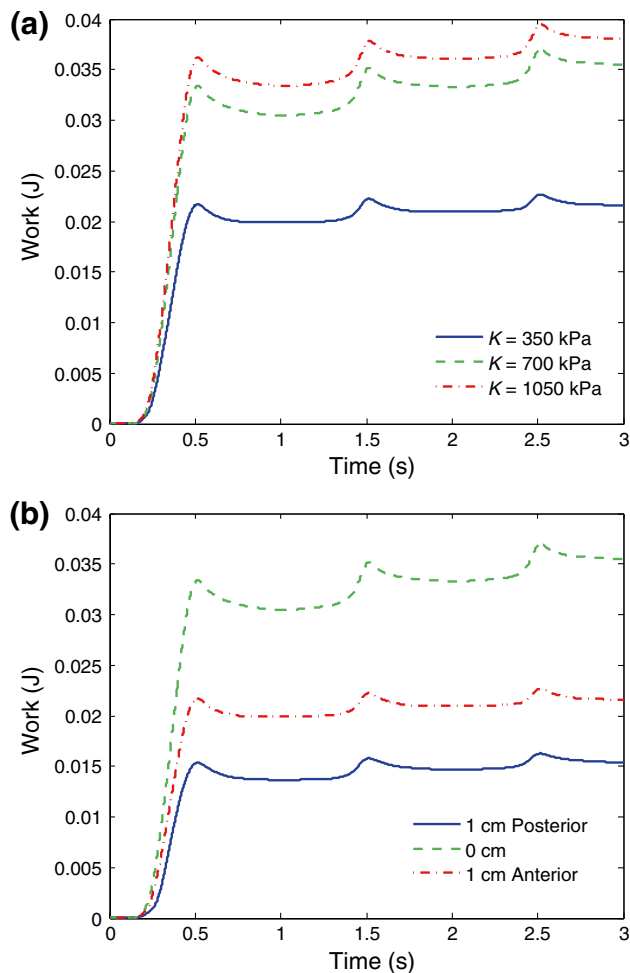


**Fig. 10** Cumulative work done during the biting of the jelly baby for (a) three variations in elastic moduli ( $K$  and  $G$ ) and (b) three variants of initial position

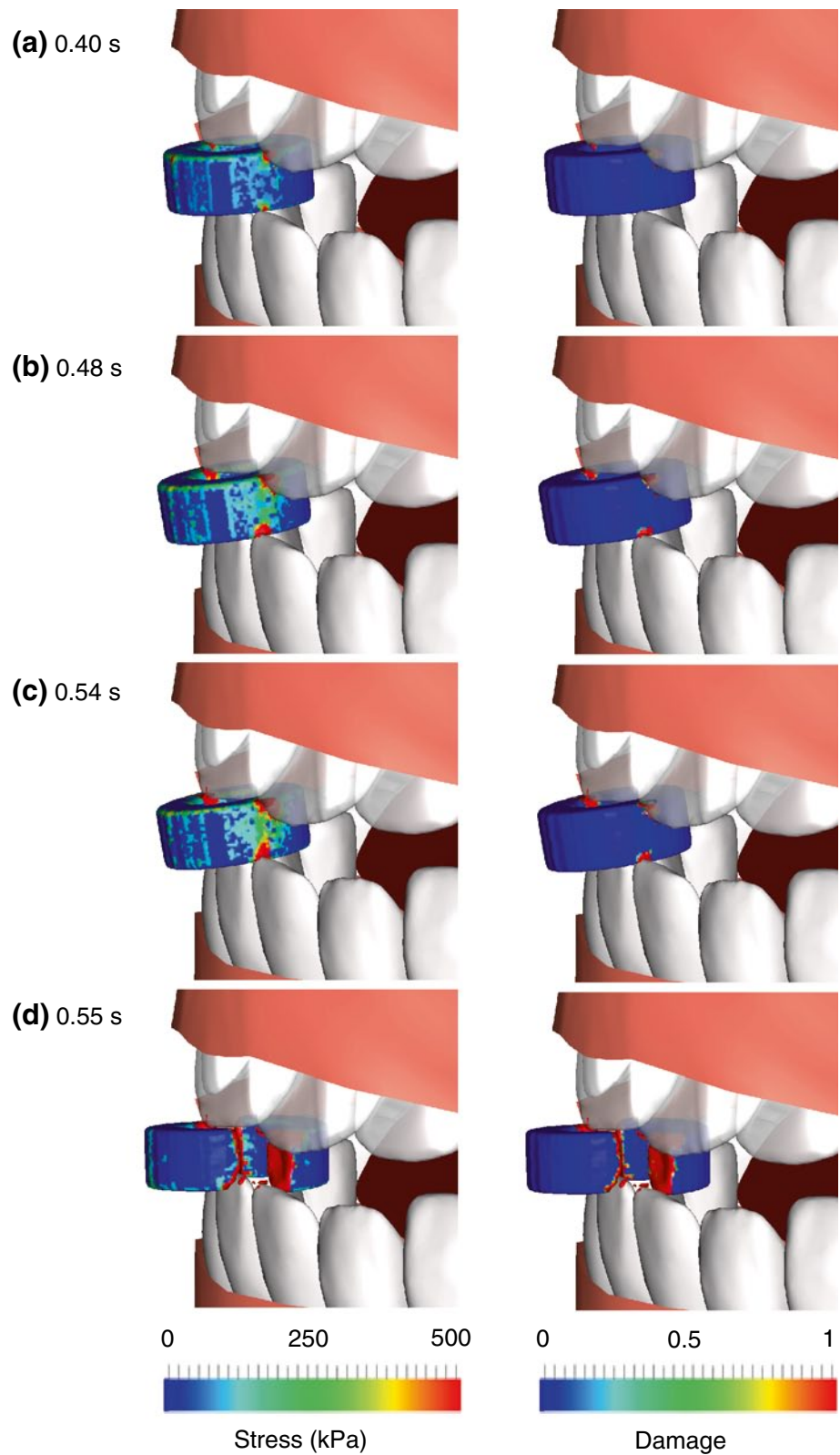
deformation occurring. This failure mode can result in a very different response under loading to that of an elastoplastic material and so requires separate consideration. The same biting configuration from “[Biting of an elastoplastic foodstuff by the incisor teeth](#)” was used, but now with a hoop-shaped brittle candy as the demonstration foodstuff. The dimensions of the mouth and brittle candy are shown in Fig. 1 (panels a and g). Three variants of flaw density,  $k$ , were used. They were  $k = 10^{26} \text{ m}^{-3}$  for the highest flawed candy,  $k = 10^{24} \text{ m}^{-3}$  for the intermediate candy and  $k = 10^{22} \text{ m}^{-3}$  for the least flawed candy. The jaw kinematics was identical to those described in “[Biting of an elastoplastic foodstuff by the incisor teeth](#)”. The foodstuff was represented by 33,700 particles with spacing of 0.2 mm, and the simulation period was 0.8 s. Simulations were run for 510 h (wall-clock) on seven cores of a Xeon E5-2650 (Intel, Santa Clara, CA, USA).

## Results and discussion

Figure 11 shows the progression of fracture of the brittle, hoop-shaped candy. The candy is coloured by von Mises stress in the left panels and the damage parameter,  $D$  (see Eq. 19), is used to colour the candy in the right panels. At 0.40 s, the teeth have contacted the candy, and a small amount of local powdering damage has occurred proximal to the area contacting the teeth. The candy shows medium levels of stress outside the region of damage, especially in the volume between the approaching top and bottom incisors. After 0.48 s, the damage has propagated a small way through the candy, but no other damage is apparent. The von Mises stress has increased between the approaching teeth, and a greater volume of material of the candy experiences higher stresses. After 0.54 s, further damage has occurred, and the stress between the approaching teeth has decreased. A small time later, after 0.55 s, the candy fails suddenly and splits into two discrete parts. The stress away from the cracks has almost completely vanished as the loading is now negligible. Unlike for the elastoplastic model (see “[Biting of an elastoplastic foodstuff by the incisor teeth](#)” and 6), the response of the candy is purely elastic, except where damage occurs and modifies the pattern of stress transmission. Again, the prediction of cracking, local damage and separation into two discrete moving fragments driven by multiple moving complex-shaped surfaces is relatively straightforward in the meshless Lagrangian framework of SPH. The movement of the jaws, teeth and candy in a mesh-based solution would require very high resolutions and adaptive remeshing. The prediction of the fracture of the foodstuff and the separation of the fragments would similarly present significant challenges in a mesh-based system.

Figure 12 shows the variation in occlusal forces and shapes of the candy during loading with variations in its flaw density,  $k$  (see Eq. 20). The candy is loaded in its starting position until about 0.25 s, when the loading causes it to rotate in the sagittal plane. This change in position relieves stress in the candy and causes the stresses in the candy to reduce markedly. The force drops to nearly zero before the candy is loaded again in its new position. All flaw density variants respond elastically in the early stages of biting (up to 0.32 s) as little damage has yet occurred. Thus, the occlusal forces for the three candy materials are very similar before 0.32 s. Microcracking initiates around the contact points with the teeth after 0.32 s. This damage reduces the capacity of the material near the microcracks to transmit tensile force and therefore reduces the force required to compress the candy. The most flawed candy therefore transmits a smaller occlusal force for the same level of compression by the teeth. Damage is minimal until 0.4 s, where a peak in occlusal force is observed. After

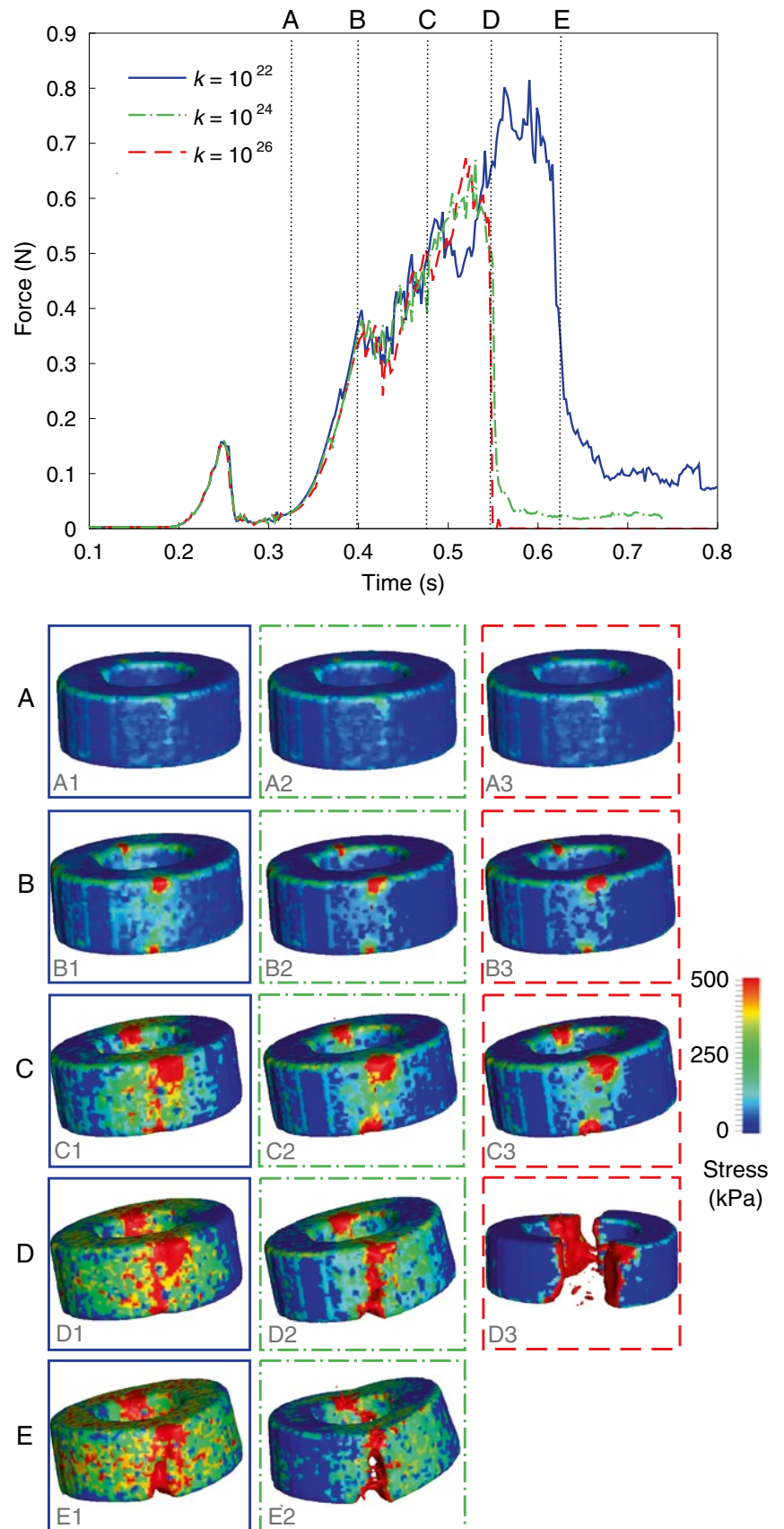
**Fig. 11** Fracture of a brittle elastic hoop-shaped candy. The candy is coloured by von Mises stress in the left panels and by damage in the right panels. Complete cracking failure of the candy occurs after 0.4 s of biting



0.4 s, significant cracking occurs and large fluctuations in occlusal force result in the candy cracks and shifts between the approaching teeth.

Occlusal forces are smaller for this case than for the previous biting one (“[Biting of an elastoplastic foodstuff by the incisor teeth](#)”) even though the candy is stiffer than the

**Fig. 12** Variation in the vertical component of occlusal force and the resultant shape of the brittle, hoop-shaped candy for different fracture properties of the candy (flaw density,  $k$ ). The candy is shown coloured by von Mises stress at four times, denoted by the letters A to E. The times for which these deformed shapes occur are indicated by the same letters on the force–time graph



jelly bean. This result is caused by the different distributions of pressure developed on each foodstuff as the top and bottom rows of teeth make contact, and the different material behaviours of each foodstuff. The jelly bean deforms to conform with the teeth when contact is made and local yielding occurs. As this deformation occurs, the contact area between the teeth and the food increases (to approximately 30 mm<sup>2</sup>). Spatially averaged pressure on the jelly bean peaked at approximately 25 kPa. However, the brittle candy does not deform significantly under load, due to a high elastic stiffness and a lack of plastic yielding. The contact area between the teeth and candy remains much smaller (approximately 5 mm<sup>2</sup>), meaning that occlusal force is small, whilst pressures on the candy are large (120 kPa). Also, because the teeth are not flat and pressure is not evenly distributed, peak pressures are larger on the candy than on the jelly bean (however, note that magnitudes of peak pressure are difficult to estimate accurately). The higher pressures on the candy lead to localised fracturing, and subsequent failure, with a modest level of occlusal force.

Once large-scale cracking has occurred, the ability of the candy to transmit tensile force diminishes greatly (even to zero, if complete failure occurs). For the most flawed candy, large cracks appear at 0.52 s, and the occlusal load drops from 0.68 N to 0.55 N (see top of Fig. 12). At 0.55 s the candy then fractures in separate pieces (see row C of Fig. 12), and the occlusal load drops from 0.55 N to 0 N. The less brittle candy does not completely separate when the first large cracks are formed. Just after 0.55 s, the intermediate candy develops large cracks that start at the top and span approximately two-thirds of its height (see row D of Fig. 12). Unlike for the most flawed candy, the occlusal load is non-zero after this fracture. This occurs because the intermediate candy has not completely separated after fracture and can still transmit a small amount of the tensile force. At 0.62 s, the least flawed candy experiences large cracks that start at the top and span almost half its height (row E of Fig. 12). The occlusal force reduces from 0.66 N at 0.616 s to 0.21 N at 0.633 s. Unlike for the other two flaw density variants, the occlusal force is significant after fracture because a large portion of the least flawed candy can still transmit tensile stress.

**Table 5** Spatially averaged (mean) and maximum von Mises stress and damage in the brittle candy during biting by the incisors at the time of fracture

Time (s)	Flaw density (m <sup>-3</sup> )	Von Mises stress (kPa)		Damage	
		Mean	Maximum	Mean	Maximum
0.63	10 <sup>22</sup>	0.9	18	0.21	1.0
0.56	10 <sup>24</sup>	0.4	12	0.11	1.0
0.55	10 <sup>26</sup>	0.2	11	0.08	1.0

Magnitudes of stress and damage at the time of fracture decrease with increased flaw density. Table 5 lists the spatially averaged and maximum values of von Mises stress and damage (*D*) in the candy at the time of failure. The most flawed candy material separates into distinct pieces at fracture (that fall away from the teeth) and therefore can no longer transmit force to the teeth. Once occlusal forces are not transmitted, the stresses in the undamaged areas of the candy decline (as also seen in row C of Fig. 12). Conversely, the least flawed material still transmits significant force to the teeth at the time of fracture and develops higher levels of stress (see again row C of Fig. 12). The maximum damage is 1.0 for all three materials since there has been complete local failure in at least one location for each material, but the spatially averaged damage across the candy decreases with increasing flaw density. The material with larger flaw densities experiences damage in a smaller volume than those with lower flaw densities where the damage is weaker but spreads over a larger volume.

Work done by the teeth during each of the simulation cases is shown in Fig. 13. A small amount is done as the candy settles in between the incisors (around 0.25 s). As it is steadily loaded (from 0.35 s onwards), the work increases approximately linearly. The work done before large-scale fracture occurs is invariant to material fracture properties. For the most flawed candy ( $k = 10^{26} \text{ m}^{-3}$ ), catastrophic fracturing occurs at 0.55 s and the work done by the teeth immediately stops increasing. As mentioned above, the intermediate candy ( $k = 10^{24} \text{ m}^{-3}$ ) does not fail completely at this time so work continues to increase modestly after this fracture. Work increases steadily for the least flawed candy ( $k = 10^{22} \text{ m}^{-3}$ ) for much longer until 0.62 s, which corresponds with the timing of significant crack growth.

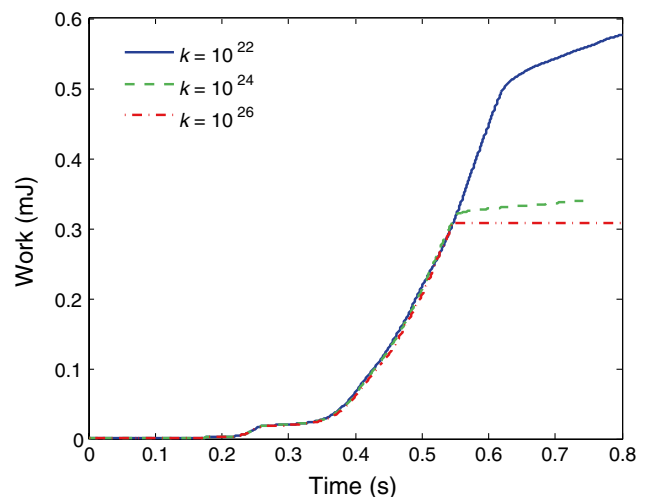


**Fig. 13** Cumulative work done during the biting of the candy for three variations in fracture properties (flaw density, *k*)

Work increases at a slower rate after this because the candy is partially fractured and occlusal force drops by about a factor of 6 (see Fig. 12) to approximately 0.1 N for the remainder of the simulation.

In summary, the flaw density in brittle foodstuffs affects the magnitude of the occlusal load during biting (for the same jaw kinematics), the work done by the teeth as cracks develop, the degree of teeth penetration required to cause catastrophic failure and the level of damage produced in the foodstuff.

## Fracture of brittle food during chewing

### Method

The fifth and final application of the model focuses on the fracture of a brittle material during chewing by the molars. Whilst many types of brittle food may be bitten by the incisors before chewing (e.g. biscuits or raw vegetables such as carrots and celery), many smaller brittle foods may be initially crushed by the molars (e.g. nuts and confectionary). The same chewing configuration and kinematics (but only one cycle) as used in “Chewing of elastoplastic food by the molars” are now used with the most brittle candy from “Fracture of brittle food from a single bite” ( $k = 10^{26} \text{ m}^{-3}$ ) to study such chewing. The brittle candy was again represented by 33,700 particles with spacing of 0.2 mm, and the simulation period was 0.5 s. Simulations were run for 140 h (wall-clock) on seven cores of a Xeon E5-2650 (Intel, Santa Clara, CA, USA).

### Results and discussion

Figure 14 shows the vertical component of occlusal force and the deformed shape of the brittle candy coloured by both von Mises stress and the damage parameter,  $D$ . The occlusal force is zero until contact is made between the top teeth and the candy at 0.25 s. It increases as the candy responds elastically to loading. At 0.305 s, the occlusal force peaks because the von Mises stress is high in the volume of the candy directly between the contact points of the top and bottom molars (see candy shape A in Fig. 14) and because damage has not yet initiated. At 0.31 s, microcracking begins at the teeth contacts (see row B in Fig. 14). Occlusal load drops immediately as microcracking damage reduces force transmission through the candy. Further elastic loading of the candy occurs without noticeably increased damage until 0.325 s. The von Mises stress has increased further in the volume of candy between the top and bottom teeth contacts (see candy shape C in Fig. 14). At 0.33 s, the microcracks combine into three large cracks and the candy fails, separating into three discrete pieces

(see row D in Fig. 14). The occlusal load drops sharply to zero as the pieces of the candy move away from the teeth and load can no longer be transmitted from the teeth. Mean damage of the candy was 0.15 at failure, which was higher than 0.10 after biting by the incisors for the same candy material. This larger value of mean damage indicates that fracturing was more intense during crushing by the molars than during biting by the incisors, which was due to the greater contact area for the molars than for the incisors.

Work done by the molars on the candy is shown in Fig. 15. Reflecting the small magnitude of force (seen in Fig. 14) between 0.25 s and 0.28 s, the work increases very slowly as the top teeth make contact with the candy and start to compress it. After 0.28 s, the force increases sharply, and the work trace shows a corresponding inflection point. However, unlike the force trace, the work increases approximately linearly until 0.33 s. After the candy fails at 0.33 s, the rate of work by the teeth is much lower. It is larger for this case (0.6 mJ) than for the biting case (0.3 mJ). This is because the contact area between the teeth and the candy is larger between the molars than for the incisors.

The simulation results show that food breakdown depends strongly on the material behaviour of the food. The brittle materials are broken down without jaw closure, whilst the elastoplastic materials require complete jaw closure to fragment the food. Whilst these material descriptions are suitable for the food types discussed in this study, many foods display more complicated behaviours that will similarly affect food breakdown. Inhomogeneous and/or anisotropic materials will deform and fracture differently if positioned differently between the teeth. Food mechanical properties also change when wetted by saliva or heated by normal body temperature inside the mouth. SPH is well suited to include these additional material behaviours, as evidenced in uses in other fields (see [24, 25]). Future work with the modelling framework will include simulation and validation of complicated food material behaviours.

## Future challenges

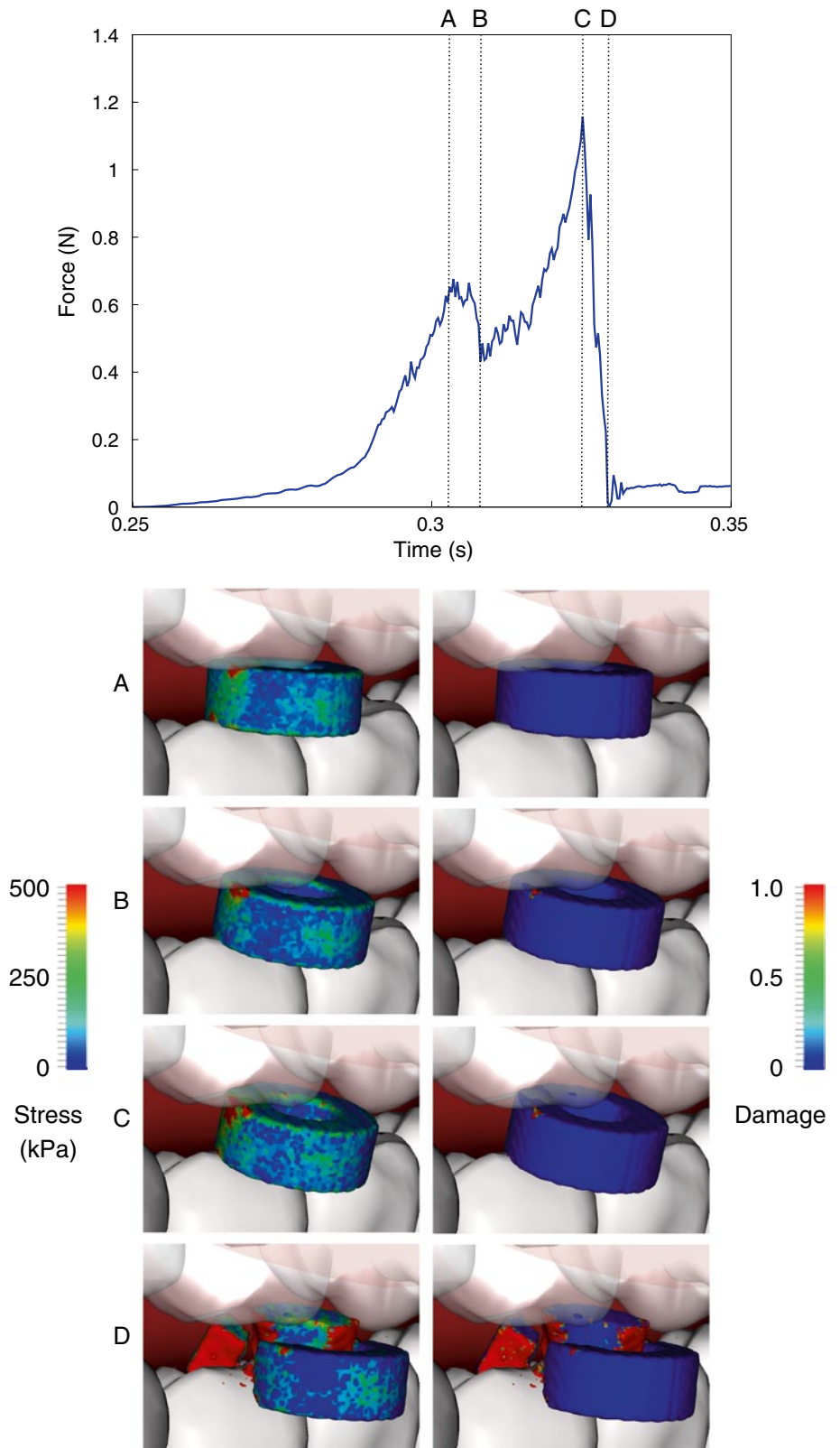
As this work is the first step in constructing a modelling framework for processes in the oral cavity during mastication, it is important to also explore the challenges that remain to be addressed and how these challenges can be addressed.

Model representation of complex solid material behaviour

Solid foods often have complicated microstructure that results in complex material behaviour. Structural



**Fig. 14** Variation in the vertical component of occlusal force and the resultant shape of the brittle, hoop-shaped candy during crushing by the molars. The deformed shape of the candy, coloured by von Mises stress in the left panels and plastic strain in the right panels, is displayed at four times, denoted by the letters *A*, *B*, *C* and *D*. The times for which these deformed shapes occur are indicated by the same letters on the force–time graph



inhomogeneity and anisotropy occurs from macro- to nano-length scales [57, 59, 98, 100], and this presents many challenges for mechanical modelling of food. Here we outline

the major steps required to simulate a large range of food structures and material behaviours in the computational framework.

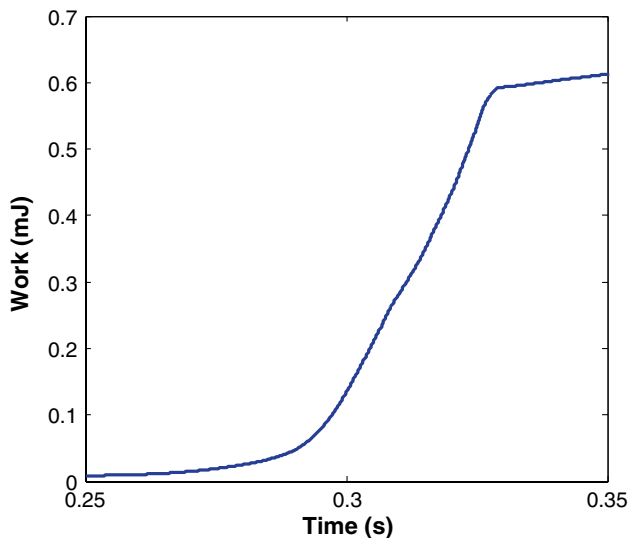


**Fig. 15** The vertical component of cumulative work done during the crushing of the candy

In many cases, the structural inhomogeneity and anisotropy are present in the macroscale, and this may be resolved by specification of differing material properties throughout the computational domain (which in the SPH context means that all the particles have different and spatially varying properties). For instance, a confectionary comprised of discrete chocolate, caramel and nut components may be represented well by specifying the mechanical properties of each component in the appropriate locations. The Lagrangian framework of a particle method such as SPH has specific advantages in modelling these variations because these material properties are attributed to specific particles which advect this information without diffusive loss during motion and breakdown in the mouth. However, in many other cases, the structural variation is at a scale that is smaller than the computational scale (which in SPH is the particle size). An example of this is an inhomogeneous distribution of voids in a food matrix that will contribute to macroscale plastic or brittle behaviour. In this case, other modelling approaches are required.

When mechanical behaviour is influenced by structural detail smaller than can be explicitly resolved by the model, one of two approaches is commonly used:

1. Homogenisation, where structural inhomogeneity is present on a small scale but large-scale structure can be represented with the use of a representative element of volume (REV). Large-scale behaviour is coupled to small-scale structural response through the assumption that the REV material behaviour is homogeneous. The stress–strain relationship for a specific REV is typically

complex, direction dependent and empirically based (therefore requiring multiple calibration constants).

2. A multiscale model approach, where coupled models at different scales link the effects of large-scale loading into micro- or nanoscale models and micro- or nanoscale structural response then influences the large-scale behaviour.

A major challenge in the homogenisation approach is the determination of an appropriate REV specification. This comprises a combination of materials characterisation (see “[Materials characterisation and validation](#)”) and modelling challenges. The REV must accurately represent the periodic structure of the food, and the stress fields must be able to be averaged on to the boundaries of the REV. A benefit of the homogenisation approach is that computational expense may be small for the level of microstructure detail that is considered. However, homogenisation can suffer from inaccuracy when the assumptions of the continuum model are broken, for instance considering fibres or cell membranes of comparative size as (or larger than) the REV, the averaging calculations will not be adequate.

Multiscale modelling involves the use of a number of models applied on different length scales. An example of this could be the prediction of compression of a polymeric matrix using one or more models of deformation of the molecular structure to inform the distribution of elastic stiffness throughout the food at a macroscale. The coupling of microscale to macroscale is an emerging area of computational modelling research, with many choices of the number, type, scale and location of microscale models and how these are coupled to the larger scale. Whilst offering the prospect of greater model fidelity by capturing much more of the fine-scale structure and its consequent behaviour, multiscale modelling is likely to add to computational expense if large numbers of microscale models are to be evaluated in transient macroscale simulations. This is a challenging process to implement but may be required when material properties are not adequately represented by the homogenisation approach.

#### Model representation of tastant transport

Once breakdown can be modelled accurately, the release of taste compounds [96] can be considered. For non-volatile tastants, which are released from food and diffuse into the saliva, models of saliva inflow and tastant diffusion are required. Saliva can be introduced into the model at the locations of the salivary ducts at flow rates suggested by experiments. The flow rate can be dynamically adjusted as chewing progresses or to suit different food material types (such as those that contain saliva stimulants, e.g. capsaicin).

The prediction of the transport of chemical species in a fluid such as saliva is a complicated multi-physics problem involving the prediction of saliva advection during interactions with moving boundaries and the diffusion of chemicals out of solid foods and within the saliva. In “Fluid motion in the anterior oral cavity”, we showed that the modelling can simulate interactions of saliva flow when interacting with moving and deforming tissues in the mouth. SPH can also be used to solve advection–diffusion equations for species transport using the formulation proposed for heat transfer by Cleary and Monaghan [17]. Model parameters may be calibrated using bench-top diffusion experiments such as those by De Loubens et al. [37] and Lauerjat et al. [66]. As the saliva fluid interacts with food solids, the tastant diffuses into the saliva phase. Sensors acting as virtual taste buds may be used to record the concentration of flavour chemical species as a function of time during chewing simulation.

#### Model representation of aroma transport

Volatile aroma compounds are released from food as the food is broken down in the mouth. The calculation of aroma transport from the food to the olfactory receptors in the nose requires the prediction of gas-phase behaviour within the trachea, oral cavity and nasal cavity. The SPH method, which is highly suited to modelling the solid and fluid phases of the processes in the oral cavity (as demonstrated in this paper), is not so well suited to simulating this gas-phase behaviour, so a one-way coupling between an SPH solid/liquid model and a grid-based method gas model (either finite volume or finite element) is likely to be a good approach.

Predicting the rate of release of aroma compounds from food fragments is a challenging problem. Volatiles are generally preferentially stored in fat and are released at a rate controlled by their lipophilicity, which is specified by their partitioning coefficient [51, 54]. The mechanical breakage of food masses controls the exposure rate and surface area of the fat phase to the gas phase and therefore the rate of volatile release. A coupled SPH-FV model would be suited to tracking both the exposed surface of the food and the transport of aroma species into and within the gas phase including sensors representing the olfactory receptors.

#### Materials characterisation and validation

The modelling challenges listed above are complicated by the need for accurate characterisation of the properties of materials when in the mouth. Food materials are often more complex than others more commonly characterised. The presence of strong inhomogeneity, anisotropy and temperature dependence of mechanical and chemical properties creates a need for intensive characterisation processes.

The microstructure of food including the size and distribution of components may be determined using imaging methods such as light microscopy, confocal laser scanning microscopy [35], high-resolution electron microscopy and light- or X-ray-scattering techniques. Mechanical characterisation such as by using uniaxial compression testing [104] and puncture testing [10] can be used to determine the mechanical response of foods during mastication. However, these techniques have not yet been applied in sufficient detail for most foods. The dependence of mechanical properties on strain rate, temperature and saliva interactions (such as absorption and lubrication) needs to be understood and quantified. Also, as mechanical properties vary between food samples, material variation may need to be characterised using statistical methods to accurately represent variation of behaviour in the mouth.

The rate at which tastants are released from food during mastication and then transported in saliva to the taste buds also needs to be characterised. Diffusion kinetics of tastant chemicals need to be measured within the solid food and in saliva in order to represent these processes quantitatively in a model [37, 66]. Viscosity and chemical composition of saliva vary greatly as food is comminuted and mixed into the liquid, but also changes significantly with the time of day and hormonal changes in the body [13]. Saliva flow rates also depend on many physiological factors and the perceived nature of the food in the mouth (e.g. dry food induces high saliva flows than a liquid food). Chemical stimuli such as capsaicin and salt affect the flow rate of saliva. The rates of saliva production need to be measured separately for each saliva duct, across a sample of the population, for successful representation in the model.

The rate of release of aroma and the speed of transport to the receptors in the nasal cavity also requires specific characterisation. The concentration of each volatile needs to be measured for each particular food, as does the statistical variation between samples. Food structure and composition controls the release rate of aroma compounds, and both static and dynamic gas flow experiments are required to measure this release rate [38]. Partitioning coefficients describe the lipophilicity of a volatile aromatic compound and therefore affect the release rate from fat within a food [66]. These coefficients may be measured specifically for a food [66] or calculated from a database of experiments [97].

Establishing confidence in model results remains a significant challenge. Food breakdown calculations may be evaluated against the measurements from *in vitro* and *in vivo* chewing experiments. Predicted occlusal force can be validated against forces measured with a materials testing system (or texture analyser), using indenter pieces with geometries similar to teeth. Calculated particle size and surface area distributions from simulations of *in vivo*

chewing experiments can be compared to measurements of expectorated material, for a range of materials and numbers of chews [71, 84]. The concentration of tastant chemicals in the mouth can be evaluated using sampling of saliva during mastication and offline determination of chemical concentrations. Likewise, model predictions of aroma concentration in the nose may be validated by measuring concentrations on the exhaled breath during *in vivo* chewing experiments [43, 44, 96].

#### Control and response of soft and hard tissues in the oral cavity

The representation of jaw, tongue, cheek and palate motion and deformation during mastication presents many challenges. The elastic behaviour of the soft and hard tissues is often anisotropic and difficult to characterise [45, 56]. Methods must strictly not produce any ill effect on the subject, for instance methods must be non-destructive and not expose the subject to dangerous levels of radiation. Also, the motion of the jaws and tongue is observed to be complicated, highly variable between subjects and linked to food structure [53]. These relationships need to be characterised over a large range of foods, and the variation between subjects needs to be determined.

Three-dimensional topographical imaging (such as MRI) provides the richest data set of soft and hard tissue positions, but is limited in spatial (1 mm) and temporal (18 Hz) resolution [93]. Electromagnetic-based motion capture can provide 3D trajectories of individual points, which is especially useful for determining jaw motion [2, 72]. Ultrasound can be used to determine soft tissue shape and position in two dimensions, which can inform the modelling of the tongue, soft palate and cheeks [8, 82]. Video fluoroscopy has been used to determine the largest simultaneous data set of soft and hard tissue positions, albeit again in two dimensions [53, 75, 81]. However, fluoroscopy is difficult to use without exposing a subject to dangerous levels of radiation. A combination of electromagnetic-based motion capture and ultrasound may be the best compromise between spatial and temporal resolution and safety.

#### Conclusions

A coupled biomechanical–SPH model was developed to investigate the breakdown of food in the oral cavity. Realistic three-dimensional geometries and motions of the jaws and tongue were incorporated into simulations of fluid flow and biting and chewing of foodstuffs. Saliva and liquid food was represented as a Newtonian fluid, and solid foodstuffs were represented as either elastoplastic or brittle elastic solids. Separate components of the oral breakdown

of food including interactions between the anatomical features of the oral cavity and liquids, chewing and biting of elastoplastic solids and biting and crushing of brittle solids were modelled. The results of the simulations provide new insights into in-mouth processing of food and establish the viability and versatility of the SPH method for this application. Modelling extensions required to predict the remaining major aspects of oral processing have been identified and can form future work with this framework.

The simulation results show that occlusal forces and the products of biting and chewing depend on the material properties of the foodstuffs. Foods with larger bulk and shear moduli generally require larger occlusal forces; however, plastic or brittle material properties also greatly affect the occlusal force required. For elastoplastic foods we found that:

- stiffer materials with the same yield stress yield earlier and display a greater amount of plastic flow for the same jaw motion,
- occlusal force and work are only modestly dependent on elastic moduli for materials with the same yield stress,
- occlusal force and work increase strongly with yield stress,
- occlusal force and work decrease when the position of food between the teeth is such that contact area is reduced.

For brittle foods with the same elastic properties, we found that:

- occlusal force and work reduce modestly when the density of flaws is higher,
- fracture occurs earlier and cracks extend further through the foodstuff when the density of flaws is higher.

Food material type affects the manner in which food is broken down. Brittle food can fail before the teeth of the upper and lower jaws make contact with each other, but elastoplastic food must be separated into discrete pieces by complete closure of the jaw.

The applications presented show the potential for coupled SPH–biomechanical models to predict the behaviour of food breakdown in the oral cavity. Measurement and modelling challenges have been identified. More complicated solid rheologies can be considered, including multi-scale modelling approaches, coupled elastic–plastic–brittle behaviour, temperature-dependent material properties and softening due to absorption by liquids such as saliva. Introduction of saliva, saliva flow and interactions with solid food need to be represented in the model. Taste release from foods and the transport of taste chemicals to the receptors need to be predicted. Likewise, the release of

volatile aroma compounds needs to be included as does the delivery of aroma chemicals to the olfactory sensors. Significant materials characterisation challenges have been outlined. As the modelling framework expands in breadth and realism, it may enhance the understanding of the complex physical and chemical interactions during mastication processes in the mouth.

**Acknowledgments** The authors would like to acknowledge the support, many helpful discussions and manuscript review by Leif Lundin, Conor Delahunty and Graham Eyres. Matthew Bolger and Fletcher Woolard are gratefully acknowledged for assistance with data processing and visualisation.

**Conflict of interest** None.

**Compliance with Ethics Requirements** This article does not contain any studies with human or animal subjects.

## References

- Agrawal KR, Lucas PW, Prinz JF, Bruce IC (1997) Mechanical properties of foods responsible for resisting food breakdown in the human mouth. *Arch Oral Biol* 42:1–9
- Agrawal KR, Lucas PW, Bruce IC (2000) The effects of food fragmentation index on mandibular closing angle in human mastication. *Arch Oral Biol* 45:577–584
- Amemiya K, Hisano M, Ishida T, Soma K (2002) Relationship between The flow of bolus and occlusal condition during mastication: computer simulation based on the measurement of characteristics of the bolus. *J Oral Rehab* 29(3):245–256. doi:10.1046/j.1365-2842.2002.00910.x
- Autodesk Maya™ software (Autodesk Inc., San Rafael, CA, USA)
- Batchelor GK (1973) An introduction to fluid dynamics. Cambridge University Press, Cambridge
- Benz W, Asphaug E (1994) Impact simulations with fracture. I. Method and Tests. *Icarus* 107(1):98–116
- Bhatka R, Throckmorton GS, Wintergerst AM, Hutchins B, Buschang PH (2004) Bolus size and unilateral chewing cycle kinematics. *Arch Oral Biol* 49(7):559–566
- Blissett A, Peinz JF, Wulfert F, Taylor AJ, Hort J (2007) Effect of bolus size on chewing, swallowing, oral soft tissue and tongue movement. *J Oral Rehabil* 34:572–582
- Bower AF (2009) Applied mechanics of solids. CRC Press, p 562
- Breuil P, Meullenet J-F (2001) A Comparison of three instrumental tests for predicting sensory texture profiles of cheese. *J Texture Stud* 32:41–55
- Brown WE, Eves D, Ellison M, Braxton D (1998) Use of combined electromyography and kinesthesiology during mastication to chart the oral breakdown of foodstuffs: relevance to measurement of food texture. *J Texture Stud* 29(2):145–167. doi:10.1111/j.1745-4603.1998.tb00161.x
- Campanella OH, Peleg M (1987) Lubricated squeezing flow of a Newtonian liquid between elastic and rigid plates. *Rheol Acta*, vol 26
- Chen J (2009) Food oral processing: a review. *Roy Soc Ch* 23:1–25
- Chen JK, Beraun JE, Jih CJ (2001) A corrective smoothed particle method for transient elastoplastic dynamics. *Comput Mech* 27(3):177–187. doi:10.1007/s004660100236
- Cleary PW (1998) Modelling confined multi-material heat and mass flows using SPH. *Appl Math Model* 22(12):981–993
- Cleary PW (2010) Elastoplastic deformation during projectile-wall collision. *Appl Math Model* 34:266–283
- Cleary PW, Monaghan JJ (1999) Conduction modelling using smoothed particle hydrodynamics. *J Comput Phys* 148:227–264
- Cleary PW, Das R (2008) The potential for SPH modelling of solid deformation and fracture. In: Reddy BD (ed) IUTAM symposium on theoretical, computational and modelling aspects of inelastic media, vol 11. IUTAM Bookseries. Springer, Netherlands, pp 287–296. doi:10.1007/978-1-4020-9090-5\_26
- Cleary PW, Prakash M (2004) Discrete-element modelling and smoothed particle hydrodynamics: potential in the environmental sciences. *Phil Trans R Soc Lond A* 362:2003–2030
- Cleary PW, Ha J, Ahuja V (2000) High pressure dies casting simulation using Smoothed Particle Hydrodynamics. *J Cast Metals Res* 12:335–355
- Cleary PW, Prakash M, Ha J, Sinnott M, Nguyen T, Grandfield J (2004) Modeling of cast systems using smoothed-particle hydrodynamics. *JOM-J Min Met Mat S* 56(3):67–70. doi:10.1007/s11837-004-0038-1
- Cleary PW, Ha J, Prakash M, Nguyen T (2006) 3D SPH flow predictions and validation for high pressure die casting of automotive components. *Appl Math Model* 30(11):1406–1427
- Cleary PW, Prakash M, Ha J (2006) Novel applications of smoothed particle hydrodynamics (SPH) in metal forming. *J Mater Process Tech* 177(1–3):41–48
- Cleary PW, Prakash M, Ha J, Stokes N, Scott C (2007a) Smooth particle hydrodynamics: status and future potential. *Prog Comput Fluid Dy* 7 (2/3/4):70–90
- Cleary PW, Pyo SH, Prakash M, Koo BK (2007) Bubbling and frothing liquids. *ACM Trans Graph* 26:97
- Cohen RCZ, Cleary PW, Mason BR (2012) Simulations of dolphin kick swimming using smoothed particle hydrodynamics. *Hum Mov Sci* 31(3):604–619
- Colagrossi A, Landrini M (2003) Numerical simulation of interfacial flows by smoothed particle hydrodynamics. *J Comput Phys* 191:448–475
- Crespo AJC, Gómez-Gesteira M, Dalrymple RA (2007) 3D SPH simulation of large waves mitigation with a dike. *J Hydraul Res* 45:631–642
- Cummins SJ, Silvester TB, Cleary PW (2012) Three-dimensional wave impact on a rigid structure using smoothed particle hydrodynamics. *Int J Num Meth Fluid* 68:1471–1496
- Dan H, Kohyama K (2007) Interactive relationship between the mechanical properties of food and the human response during the first bite. *Arch Oral Biol* 52(5):455–464
- Das R, Cleary PW (2010) Effect of rock shapes on brittle fracture using Smoothed Particle Hydrodynamics. *Theor Appl Fract Mec* 53:47–60
- Das R, Cleary PW (2013) A mesh-free approach for fracture modelling of gravity dams under earthquake. *Int J Fract* 179:9–33
- Das R, Cleary PW (2013b) Simulation of uniaxial compression tests and stress wave propagation using smoothed particle hydrodynamics. *Int J Numer Anal Met* (under review)
- Das AK, Das PK (2009) Bubble evolution through submerged orifice using smoothed particle hydrodynamics: basic formulation and model validation. *Chem Eng Sci* 64:2281–2290
- Day L, Xu M, Øiseth S, Hemar Y, Lundin L (2010) Control of morphological and rheological properties of carrot cell wall particle dispersions through processing. *Food Bioprocess Technol* 3:928–934
- De Leffe M, Le Touzé D, Alessandrini B (2010) SPH modeling of shallow-water coastal flows. *J Hydraul Res* 48:118–125

37. De Loubens C, Panouillé M, Saint-Eve A, Délérís I, Tréléa IC, Souchon I (2011) Mechanistic model of in vitro salt release from model dairy gels based on standardized breakdown test simulating mastication. *J Food Eng* 105:161–168
38. de Roos KB (2003) Effect of texture and microstructure on flavour retention and release. *Int Dairy J* 13:593–605
39. Dejak B, Mlotkowski A, Romanowicz M (2003) Finite element analysis of stresses in molars during clenching and mastication. *J Prosthet Dent* 90(6):591–597
40. Dickie AM, Kokini JL (1983) An improved model for food thickness from non-Newtonian fluid mechanics in the mouth. *J Food Sci* 48(1):57–61
41. Drewnowski A, Shrager EE, Lipsky C, Stellar E, Greenwood MRC (1989) Sugar and fat: sensory and hedonic evaluation of liquid and solid foods. *Physio Behav* 45(1):177–183
42. Ellero M, Kröger M, Hess S (2002) Viscoelastic flows studied by smoothed particle dynamics. *J Non-Newton Fluid* 105(1):35–51
43. Frank D, Appelqvist I, Piyasiri U, Wooster TJ, Delahunty C (2011) Proton transfer reaction mass spectrometry and time intensity perceptual measurement of flavour release from lipid emulsions using trained human subjects. *J Agric Food Chem* 59:4891–4903
44. Frank DC, Eyres GT, Piyasiri U, Delahunty CM (2012) Effect of food matrix structure and composition on aroma release during oral processing using in vivo monitoring. *Flavour Fragr J* 27:433–444
45. Gerard JM, Ohayon J, Luboz V, Perrier P, Payan Y (2005) Non-linear elastic properties of the lingual and facial tissues assessed by indentation technique: application to the biomechanics of speech production. *Med Eng Phys* 27:884–892
46. Gomez-Gesteira M, Rogers BD, Dalrymple RA, Crespo AJC (2010) State-of-the-art of classical SPH for free-surface flows. *J Hydraul Res* 48:6–27
47. Grady DE, Kipp ME (1980) Continuum modelling of explosive fracture in oil shale. *Int J Rock Mech Min* 17(3):147–157
48. Gray JP, Monaghan JJ, Swift RP (2001) SPH elastic dynamics. *Comput Methods Appl Mech Eng* 190(49–50):6641–6662
49. Guzel BU, Prakash M, Semercigil E, Turan O (2005) Energy dissipation with sloshing for absorber design. *ASME conference proceedings 2005* (42169):1807–1814
50. Ha J, Cleary PW (2000) Comparison of SPH simulations of high pressure die casting with the experiments and VOF simulations of Schmid and Klein. *Int J Cast Metal Res* 12:409–418
51. Harrison M, Campbell S, Hills BP (1998) Computer simulation of flavour release from solid foods in the mouth. *J Agric Food Chem* 46:2736–2743
52. Hiiemae KM, Palmer JB (2003) Tongue movements in feeding and speech. *Crit Rev Oral Biol M* 14(6):413–429. doi:10.1177/154411130301400604
53. Hiiemae K, Heath MR, Heath G, Kazazoglu E, Murray J, Sapper D, Hamblett K (1996) Natural bites, food consistency and feeding behaviour in man. *Arch Oral Biol* 41:175–189
54. Hills BP, Harrison M (1995) Two-film theory of flavour release from solids. *Int J Food Sci Technol* 30:425–436
55. Hilton JE, Cleary PW (2012) A multiscale method for geophysical flow events. *J Multiscale Comp Eng* 10(4):375–390
56. Huang Y, White DP, Malhotra A (2007) Use of computational modelling to predict responses to upper airway surgery in obstructive sleep Apnea. *Laryngoscope* 117:648–653
57. Hutchinson RJ, Simms I, Smith AC (1988) Anisotropy in the mechanical properties of extrusion cooked maize foams. *J Mater Sci Lett* 7:666–668
58. Johnsen SE, Trulsson M (2005) Encoding of amplitude and rate of tooth loads by human periodontal afferents from premolar and molar teeth. *J Neurophysiol* 93:1889–1897
59. Khan AA, Vincent JFV (1993) Anisotropy in the fracture properties of apple flesh as investigated by crack-opening tests. *J Mater Sci* 28:45–51
60. Kohyama K, Nishi M (1997) Direct measurement of biting pressures for crackers using a multiple-point sheet sensor. *J Texture Stud* 28(6):605–617. doi:10.1111/j.1745-4603.1997.tb00141.x
61. Kohyama K, Hatakeyama E, Dan H, Sasaki T (2005) Effects of sample thickness on bite force for raw carrots and fish gels. *J Texture Stud* 36(2):157–173. doi:10.1111/j.1745-4603.2005.00009.x
62. Kokini JL, Kadane JB, Cussler EL (1977) Liquid texture perceived in the mouth. *J Texture Stud* 8(2):195–218
63. Koolstra JH, van Eijden TMGJ (2005) Combined finite-element and rigid-body analysis of human jaw joint dynamics. *J Biomech* 38(12):2431–2439
64. Koriath TWP, Romilly DP, Hannam AG (1992) Three-dimensional finite element stress analysis of the dentate human mandible. *Am J Phys Anthropol* 88(1):69–96
65. Lassauzay C, M-As Peyron, Albuissou E, Dransfield E, Woda A (2000) Variability of the masticatory process during chewing of elastic model foods. *Eur J Oral Sci* 108(6):484–492
66. Lauerjat C, Délérís I, Tréléa IC, Salles C, Souchon I (2009) Salt and Aroma compound release in model cheeses in relation to their mobility. *J Agric Food Chem* 57:9878–9887
67. Lepley C, Throckmorton G, Parker S, Buschang PH (2009) Masticatory performance and chewing cycle kinematics: are they related? *Angle Orthod* 80(2):295–301. doi:10.2319/061109-333.1
68. Libersky L, Petschek A (1991) Smooth particle hydrodynamics with strength of materials. In: Trease H, Fritts M, Crowley W (eds) *Advances in the free-Lagrange method including contributions on adaptive gridding and the smooth particle hydrodynamics method*, vol 395. *Lecture Notes in Physics*. Springer, Berlin, pp 248–257. doi: 10.1007/3-540-54960-9\_58
69. Limido J, Espinosa C, Salaün M, Lacombe JL (2007) SPH method applied to high speed cutting modelling. *Int J Mech Sci* 49:898–908
70. Liu MB, Liu GR, Lam KY, Zong Z (2003) Smoothed particle hydrodynamics for numerical simulation of underwater explosion. *Comput Mech* 30(2):106–118. doi:10.1007/s00466-002-0371-6
71. Lucas PW, Luke DA (1986) Is food particle size a criterion for the initiation of swallowing? *J Oral Rehabil* 13:127–136
72. Lucas PW, Ow RKK, Ritchie GM, Chew CL, Keng SB (1986) Relationship between jaw movement and food breakdown in human mastication. *J Dental Res* 65:400–404
73. Mathmann K, Kowalczyk W, Delgado A (2009) Development of a hybrid model predicting the mouthfeel of yogurt. *J Texture Stud* 40:16–35
74. Melosh HJ, Ryan EV, Asphaug E (1992) Dynamic fragmentation in impacts: hydrocode simulation of laboratory impacts. *J Geophys Res* 97:14735–14759
75. Mioche L, Hiiemae KM, Palmer JB (2002) A postero-anterior videofluorographic study of the intra-oral management of food in man. *Arch Oral Biol* 47:267–280
76. Monaghan JJ (1994) Simulating free surface flows with SPH. *J Comput Phys* 110(2):399–406
77. Monaghan JJ (2000) SPH without a tensile instability. *J Comput Phys* 159(2):290–311
78. Monaghan JJ (2005) Smoothed particle hydrodynamics. *Rep Prog Phys* 68:1703–1759
79. Nicosia MA, Robbins J (2001) The fluid mechanics of bolus ejection from the oral cavity. *J Biomech* 34(12):1537–1544
80. Oger G, Doring M, Alessandrini B, Ferrant P (2006) Two-dimensional SPH simulations of wedge water entries. *J Comput Phys* 213:803–822

81. Palmer JB, Hiiemae KM, Liuf J (1997) Tongue-jaw linkages in human feeding: a preliminary videofluorographic study. *Arch Oral Biol* 42:429–441
82. Peng C-L, Jost-Brinkmann P-G, Yoshida N, Chou H-H, Lin C-T (2004) Comparison of tongue functions between mature and tongue-thrust swallowing: an ultrasound investigation. *Am J Orthod Dentof Ac* 125:562–570
83. Peyron M-A, Mioche L, Renon P, Abouelkaram S (1996) Masticatory jaw movement recordings: a new method to investigate food texture. *Food Qual Prefer* Second Rose Marie Pangborn Memorial Symposium 7(3–4):229–237
84. Peyron M-A, Mishellany A, Woda A (2004) Particle size distribution of food boluses after mastication of six natural foods. *J Dent Res* 83:578–582
85. Prakash M, Cleary PW, Ha J, Noui-Mehidi MN, Blackburn HM (2007a) Simulation of suspension of solids in a liquid in a mixing tank using SPH and comparison with physical modelling experiments. *Prog Comput Fluid Dy* 7 (2/3/4):91–100
86. Prakash M, Cleary PW, Grandfield J, Rohan P, Nguyen V (2007) Optimisation of ingot casting wheel design using SPH simulations. *Prog Comput Fluid Dy* 7(2–4):101–110
87. Rantonen PJF, Meurman JH (1998) Viscosity of whole saliva. *Acta Odontol Scand* 56:210–214
88. Robinson M, Cleary PW, Monaghan J (2008) Analysis of mixing in a Twin Cam mixer using smoothed particle hydrodynamics. *Am Inst Chem Eng J (AIChEJ)* 54:1987–1998
89. Röhrle O, Pullan AJ (2007) Three-dimensional finite element modelling of muscle forces during mastication. *J Biomech* 40(15):3363–3372
90. Rudman M, Cleary PW, Prakash M (2009) Simulation of liquid sloshing in a model LNG tank using smoothed particle hydrodynamics. *Int J Offshore Polar* 19(4):286–294
91. Souto Iglesias A, Pérez Rojas L, Zamora Rodríguez R (2004) Simulation of anti-roll tanks and sloshing type problems with smoothed particle hydrodynamics. *Ocean Eng* 31:1169–1192
92. Stellingwerf RF, Wingate CA (1993) Impact modeling with smooth particle hydrodynamics. *Int J Impact Eng* 14(1–4):707–718
93. Stone M, Davis EP, Douglas AS, NessAiver M, Gullapalli R, Levine WS, Lundberg A (2001) Modeling the motion of the internal tongue from tagged cine-MRI images. *J Acoust Soc Am* 109:2974–2982
94. Sun Y, Xu WL (2010) Simulation of food mastication based on discrete element method. *Int J Comput Appl T* 39 (1/2/3):3–11
95. Swegle JW, Attaway SW (1995) On the feasibility of using Smoothed Particle Hydrodynamics for underwater explosion calculations. *Comput Mech* 17(3):151–168. doi:10.1007/bf00364078
96. Taylor AJ (2002) Release and transport of flavours in vivo: physicochemical, physiological, and perceptual considerations. *Compr Rev Food Sci Food Saf* 1:45–57
97. Tetko IV, Gasteiger J, Todeschini R, Mauri A, Livingstone D, Ertl P, Palyulin VA, Radchenko EV, Zefirov NS, Makarenko AS, Tanchuk VY, Prokopenko VV (2005) Virtual computational chemistry laboratory: design and description. *J Comput Aid Mol Des* 19:453–463
98. Ubbink J, Burbidge A, Mezzenga R (2008) Food structure and functionality: a soft matter perspective. *Soft Matter* 4:1569–1581
99. Van Der Bilt A, Tekamp A, Van Der Glas H, Abbink J (2008) Bite force and electromyography during maximum unilateral and bilateral clenching. *Eur J Oral Sci* 116:217–222
100. van Hecke E, Allaf K, Bouvier JM (1995) Texture and structure of crispy-puffed food products I: mechanical properties in bending. *J Texture Stud* 26:11–25
101. Wilkins ML (1964) Calculation of elastic-plastic flow. In: *Methods of computational physics*, vol 8. Academic Press, New York, pp 211–263
102. Wilkinson C, Dijksterhuis GB, Minekus M (2000) From food structure to texture. *Trends Food Sci Tech* 11(12):442–450
103. Williams SH, Wright BW, Truong V, Daubert CR, Vinyard CJ (2005) Mechanical properties of foods used in experimental studies of primate masticatory function. *Am J Primatol* 67(3):329–346
104. Wium H, Qvist KB, Gross M (1997) Uniaxial compression of UF-Feta cheese related to sensory texture analysis. *J Texture Stud* 28:455–476
105. Xu X, Yuan S (2011) An examination of the force generated from incisor penetration into foods with different textural properties part I: experimental observation. *J Texture Stud* 42(3):228–235. doi:10.1111/j.1745-4603.2011.00295.x
106. Yashiro K, Takada K (2005) Model-based analysis of jaw-movement kinematics using jerk-optimal criterion: simulation of human chewing cycles. *J Electromyogr Kines* 15(5):516–526